Earth Planet. Sci. Lett. 645 (2024) 118930

Contents lists available at ScienceDirect

Earth and Planetary Science Letters

journal homepage: www.elsevier.com/locate/epsl

The helium and carbon isotopic signature of Ocean island basalts: Insights from Fogo volcano (Cape Verde archipelago)

Francesco Maria Lo Forte [a], Guillaume Boudoire [b,c], Maria Luce Frezzotti [d], Silvio Giuseppe Rotolo [a,c], Andres Sandoval-Velasquez [a], Fátima Viveiros [e], Vittorio Zanon [e], Alessandro Aiuppa [a], Andrea Luca Rizzo [d,f,*]

[a] Dipartimento di Scienze della Terra e del Mare, Università degli Studi di Palermo, Palermo 90123, Italy
[b] Université Clermont Auvergne, CNRS, IRD, OPGC, Laboratoire Magmas et Volcans, F-63000 Clermont-Ferrand, France
[c] Istituto Nazionale di Geofisica e Vulcanologia, Sezione di Palermo, Via Ugo La Malfa 153, 90146 Palermo, Italy
[d] Dipartimento di Scienze dell'Ambiente e della Terra, Università degli Studi di Milano-Bicocca, Piazza della Scienza 4, 20126 Milano, Italy
[e] Instituto de Investigação em Vulcanologia e Avaliação de Riscos, Universidade dos Açores, Rua Mãe de Deus, Ponta Delgada PT-9500-321, Portugal
[f] Istituto Nazionale di Geofisica e Vulcanologia, Sezione di Milano, Via Alfonso Corti 12, 20133 Milano, Italy

ARTICLE INFO

Editor: Dr Fang-Zhen Teng

Keywords:
Ocean island basalts
Pico do Fogo
Fluid inclusions
Magmatic degassing
Mantle source
Geodynamics

ABSTRACT

Fluid inclusions (FI) entrapped in phenocrysts carried by Ocean Island Basalts (OIB) contain key information on volatiles' abundance and origin in their mantle sources. Here, we add new piece of knowledge to our understanding of volatile geochemistry in global OIB magmas, by presenting new noble gas (He-Ne-Ar) and carbon (C) isotope results for olivine- and clinopyroxene-hosted FI from enclaves, lavas, tephra and volcanic gas samples from Fogo, the only frequently active volcano at the Cape Verde archipelago (eastern Atlantic Ocean). FI, together with crater fumaroles, constrain the Fogo $^{3}He/^{4}He$ signature at 7.14–8.44 R_c/R_a (where R_C is the air-corrected $^{3}He/^{4}He$ isotope ratio, and R_a is the same ratio in air), which is within the typical MORB (Mid-Ocean Ridge Basalt) mantle. The carbon isotopic ratio ($\delta^{13}C$ vs. Pee Dee Belemnite) of CO_2 in FI and fumaroles range from -6.04 to -4.41 ‰. We identify systematic variations of $\delta^{13}C$ and He/Ar* with FI entrapment pressure (estimated from a combination of host mineral barometry and FI microthermometry), from which we develop a model for volatile degassing in the mantle-to-crustal magma storage system. The model predicts a crustal-like signature for carbon ($\delta^{13}C$ of -0.4 ± 1.0 ‰) in primary melts formed by mantle melting at ~2200 MPa (~77 km) and a source He/Ar* ratio of 0.90–0.24, which are indicative of variably depleted mantle metasomatized by carbon enriched melts/fluids from a crustal component. We also use our results to characterise regional (in the Cape Verde and Canary archipelagos) and global trends in C and He isotope composition from OIB. From a comparison with the few other OIB localities for which $\delta^{13}C$ are available, we propose that a carbon enriched crustal component could be recurrent at a global scale in OIB magmatism, although often masked by isotope fractionation during magmatic degassing. We additionally find that, at regional scale, He isotopes in OIB scale inversely correlate with the degree of partial melting of the mantle beneath individual islands' (inferred from the La/Yb ratio of erupted basalts). More widely, our results corroborate previously established global relationships between OIB He isotopic signature, plume buoyancy flux and overlying plate velocity. In this interpretation, the MORB-like $^{3}He/^{4}He$ (8 ± 1 Ra) at Fogo reflects a combination of (i) low to medium magma productivity, (ii) relatively low plume buoyancy flux (~1.1 Mg/s), and (iii) slow average velocity (~3 cm/yr) of the overlying plate.

1. Introduction

Ocean Island Basalts (OIB) offer invaluable insights into the geochemistry of the Earth's upper mantle, and on the characteristics of deeply rooted mantle plumes (Kurz et al., 1996; Hoernle et al., 2000). OIB are, for example, known to exhibit highly variable radiogenic

* Corresponding author at: Dipartimento di Scienze dell'Ambiente e della Terra, Università degli Studi di Milano-Bicocca, Piazza della Scienza 4, 20126 Milano, Italy.
E-mail address: andrealuca.rizzo@unimib.it (A.L. Rizzo).

https://doi.org/10.1016/j.epsl.2024.118930
Received 13 March 2024; Received in revised form 29 July 2024; Accepted 2 August 2024
Available online 22 August 2024

isotope (Sr-Nd-Pb) signatures, commonly interpreted as evidence of mantle heterogeneity (e.g., Jackson and Dasgupta, 2008), and to reflect the existence of several distinct mantle isotopic components interacting each other, and mixing in various proportions, in the various OIB localities (Zindler and Hart, 1986; Jackson et al., 2017a; Stracke et al., 2019).

Noble gases, due to their chemical inertness, behave as strongly incompatible elements during mantle partial melting. The ^{3}He and ^{4}He isotopes have primordial and radiogenic origin, respectively (Ozima and Podosek, 2002), and because they do not fractionate one each other during mantle melting and degassing, they can – at least in principle - accurately record the signature of the mantle source (e.g., Boudoire et al., 2018; Rizzo et al., 2018; Sandoval-Velasquez et al., 2021a, b). The utility of light noble gases (He, Ar and Ne) as tracers of mantle processes (e.g., Dunai and Porcelli, 2002; Boudoire et al., 2018, 2020; Rizzo et al., 2018, 2021; Day et al., 2022; Sandoval-Velasquez et al., 2023) stems from the distinct isotopic signatures of fluid components (primordial, crustal, radiogenic, atmospheric) potentially involved in the OIB mantle source. These signatures can be reconstructed from the analysis of fluid inclusions (FI) in the minerals of lavas and xenoliths (e.g., Day et al., 2022) that have not interacted with crustal fluids. FI have revealed especially useful for understanding the processes that modify the characteristics of the mantle in space and time, and the nature and signature of fluids in the mantle (Frezzotti et al., 1992, 2002; Frezzotti and Peccerillo, 2004). Past studies (e.g., Gautheron et al., 2005; Boudoire et al., 2018, 2020; Rizzo et al., 2018, 2021; Sandoval-Velasquez et al., 2021a, 2021b, 2023) have identified large regional and global diversity in noble gas isotopic compositions in FI. However, the factors responsible for the observed variability are not entirely understood (Day et al., 2022).

In the Cape Verde archipelago, notable noble gas heterogeneities have been identified (Christensen et al., 2001; Doucelance et al., 2003; Mourão et al., 2012) (Figs. 1,2). By combining noble gas with radiogenic isotopes, heterogeneities have been interpreted either as due to mixing of different mantle components (e.g., Gerlach et al., 1988), or as the result of the interaction of the "mantle plume" with several shallow lithospheric components, such as carbonatites, MORB-type mantle, and oceanic crust (Millet et al., 2008). He isotope data from seven out of the 10 islands span from < 1 Ra (where R is the ^{3}He/^{4}He isotopic ratio of the sample and Ra is the corresponding ratio in air) to > 40 Ra (Fig. 1) (Christensen et al., 2001; Doucelance et al., 2003; Mourão et al., 2012). Large inter-island isotopic diversity and intra-island heterogeneity is observed (Fig. 1). The least radiogenic (more primitive mantle-like) He compositions is observed at São Nicolau (10.5–15.7 Ra; mean, 13.3 Ra) and in the northern islands in general (3.2–42.6 Ra, mean 11.4 Ra) (Fig. 2), and more MORB-like (8 ± 1 Ra; Graham, 2002) compositions in the southern islands of Santiago (0.2–29.3 Ra; mean 8.1 Ra) and Fogo (3.7–12.1 Ra; mean 7.9 Ra) (Christensen et al., 2001; Doucelance et al., 2003; Mourão et al., 2012; Alonso et al., 2021; Melián et al., 2021). At Fogo Island, the only active island, the He isotope compositions measured in FI and in crater fumaroles range from 3.7 to 12.1 Ra (Doucelance et al., 2003; Alonso et al., 2021; Melián et al., 2021).

Relative to noble gases, the carbon isotope signature of OIB (and of their mantle sources) has been more difficult to decipher. This is because very few FI results are available (Aubaud, 2022), and because of the technical challenges in precise determinations of δ^{13}C compositions of dissolved carbon in glassy melt inclusions and in FI in magmatic minerals. Yet we know from FI in mantle xenoliths (Deines, 2002) that the mantle at a global scale has diverse carbon isotope signatures, with δ^{13}C values ranging from −29.9 ‰ in Hawaii (Pineau and Mathez, 1990) to +0.9 ‰ at El Hierro (Canary Islands, Sandoval-Velasquez et al., 2021a). This wide range reflects a combination of (i) isotopic fractionation during magmatic degassing (e.g., Aubaud, 2022), and (ii) mixing of crustal carbon components, ranging from organic carbon (−30 ‰ to −10 ‰) to limestone (from −1 ‰ to +1 ‰), with Depleted MORB Mantle (DMM) carbon (δ^{13}C of −4 to −8 ‰) (Sano and Marty, 1995; Deines, 2002). OIBs are carbon-rich (Sun and Dasgupta, 2023 and references therein), indicating these magmas do form by low-degree partial melting of carbon-enriched (metasomatized) mantle sources. Measuring the carbon isotopes of alkaline OIB is thus critical for testing models (Dasgupta, 2018) that see carbonatitic to carbonated silicate melts metasomatic agents to derive from melting of deeply subducted, carbon enriched crustal lithologies. The presence of recycled crustal carbon in OIB mantle source has recently been identified in the Canary Islands (Sandoval-Velasquez et al., 2021a, 2023), but remains untested in most OIB localities including at Cape Verde, where carbon isotopic results are only available for Fogo fumaroles (Melián et al., 2021).

Here, we present new noble gas (He-Ne-Ar) isotopic data in FI from crystals in lavas, tephra, and enclaves from Fogo volcano, including the first FI carbon isotopic measurements for the Cape Verde archipelago. We interpret our results in the regional and global OIB context in the attempt to refine our understanding of the factors that primarily control the OIB isotopic diversity. The carbon isotope ratios are used to model the source-to-surface carbon isotopic evolution during magmatic degassing in the volcano storage system, revealing the presence of a recycled carbon rich crustal component in the mantle, source for OIB volcanism.

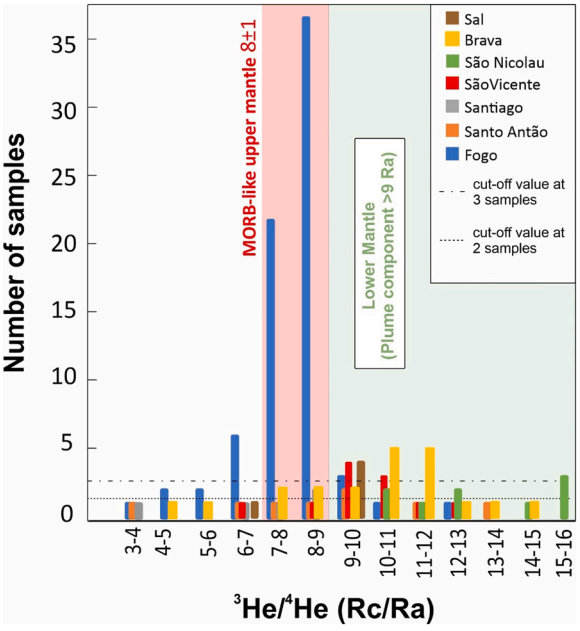

Fig. 1. He isotopes (expressed as Rc/Ra values, where Rc is the air-corrected He isotope composition) in FI and fumarolic gases from the different islands of Cape Verde archipelago. For FI, for consistency with our analytical approach, we considered only samples analysed by single-step crushing. Data are from Christensen et al. (2001), Doucelance et al. (2003), Mourão et al. (2012), Alonso et al. (2021), Melián et al. (2021). Measurements are categorised in 19 different classes. Two different cut-off values (of a minimum of 2 and 3 samples per class) are proposed (for the less and more populated classes, respectively); samples/classes below these cut-off values are considered outliers, and are not treated in the calculation of individual islands' refined ranges of Rc/Ra values, shown in Fig. 2. No data is available for Maio and Boa Vista islands.

2. Volcanological and geodynamical background

Cape Verde archipelago stands on the Cape Verde Rise, an oceanic intraplate bathymetric anomaly, interpreted to result from the interaction between a mantle plume and the African plate, moving at an average velocity of~ 3 cm/yr (Hoggard et al., 2020 and reference therein). The archipelago consists of ten major islands divided into two main branches: the northern islands (Santo Antão, São Vicente, Santa Luzia, São Nicolau, Sal, and Boa Vista), and the southern islands (Maio, Santiago, Fogo and Brava). The two branches exhibit contrasting

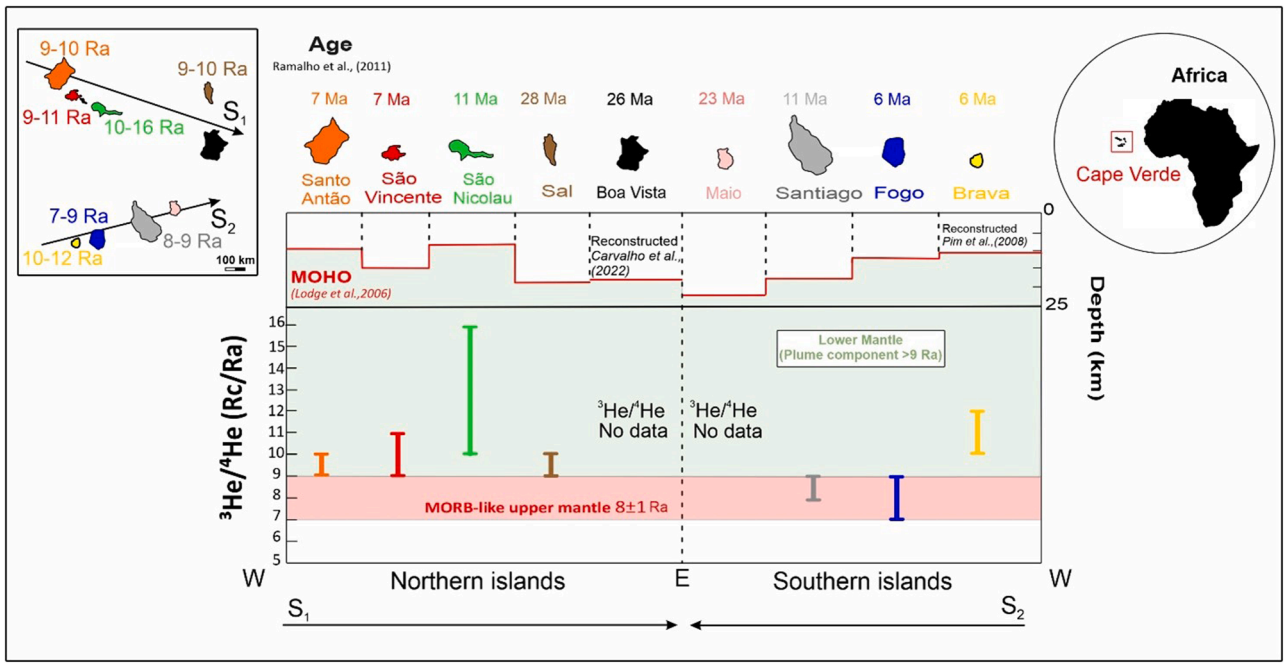

Fig. 2. The $^{3}He/^{4}He$ defined ranges for individual islands of the Cape Verde archipelago. We initially screened the entire dataset available (listed in Table S1 of the Supplementary material S1) and performed a data quality check that considers the noble gas extraction method used (single-step and multi-step crushing, and melting). We discarded all results employing multi-step crushing or melting extraction methods that, in contrast to the single-step crushing (employed by Gautheron et al., 2005), are more prone to release the radiogenic and cosmogenic component of helium trapped within the crystal lattice. Insets show position of the archipelago relative to Africa (right) and the southern and northern branches (left). The reported ages are the maximum ages reported for each island from Ramalho (2011). The solid red line is Moho depth (data from Lodge and Helffrich, 2006 except for Boa Vista, where the Moho depth is based on the reconstruction of Carvalho et al. (2022), and Brava, based on the Moho reconstruction of Pim et al. (2008)).

isotopic (Sr-Nd-Pb) signature, with HIMU (High-μ=high $^{238}U/^{204}Pb$ ratio) and EM-I (Enriched Mantle) mantle source affinities (Gerlach et al., 1988; Doucelance et al., 2003; Mata et al., 2017). Recent melt inclusion work evidenced the presence of 342–411 ppm carbon in the local mantle source (Lo Forte et al., 2024). A carbon-rich, metasomatized mantle source is additionally supported by rare carbonatites, which have been erupted both in southern islands of Fogo (Hoernle et al., 2002), Brava (Mourão et al., 2010) and Santiago (Martins et al., 2010), and in the northern island of Sal (Bonadiman et al., 2005) and São Vicente (Jørgensen and Holm, 2002).

Magmatism at Fogo Island dates back at 3–4.5 Ma (Day et al., 1999) and is dominated by silica-undersaturated magmas (Gerlach et al., 1988) and rare carbonatites (e.g., Hoernle et al., 2002; Mourão et al., 2012). Previous studies (e.g., Hildner et al., 2011, 2012; Mata et al., 2017; Klügel et al., 2020; Lo Forte et al., 2023) on Fogo focused on reconstructing the magma storage system, which is thought to consist of: (i) a deep magma reservoir at 27–36 km depth, (ii) a main magma storage zone at ~12–24 depth, (iii) and a magma stagnation zone at ~9–12 km depth.

3. Methods

3.1. Samples

We report on the He, Ne, Ar, and CO_2 isotope signature of FI in olivine and clinopyroxene crystals from lavas, tephra and mafic enclaves from Fogo Island. We refer to enclaves, rather than xenoliths, as they have been found to be formed from the same or different magmas at Fogo through various magmatic processes (see Section 5.1 and Supplementary Material S1). Lavas and tephra samples have been already studied for bulk-rock and melt inclusion geochemistry, and FI microthermometry (Lo Forte et al., 2023; 2024) and their data are summarized in Section 3.1. The mafic enclaves (FG1-A, FG2-A1, FG2-A3, FG3-A, FG4-A, FG4-B, FG4-D, and FG4-E) were found in lavas and tephra outcropping in the periphery of Pico do Fogo and within the Chã das Caldeiras summit depression (Table 1), as already reported in a previous study by Barker et al. (2023). The enclaves are made mostly of crystals of clinopyroxene and olivine, with minor amount of plagioclase and Fe-Ti oxides, so they can be roughly classified as clinopyroxenite or olivine-clinopyroxenite.

We also report new isotopic data for two Pico do Fogo fumarole samples (PF-1 and PF-2), whose chemical composition and SO_2 flux are reported in Aiuppa et al. (2020). Table 1 lists the studied samples and summarizes the analyses conducted. Further details on the lava, tephra, and mafic enclaves, as well as the analytical methods employed for the FI composition and CO_2 densimetry (Raman spectroscopy) and mineral chemistry (Electron Microprobe, EMPA), are provided in Supplementary Material S2. Based on their compositions, clinopyroxene crystals in mafic enclaves are categorised in Group Ia, Ib and II (see Supplementary Material S2).

3.2. Noble gases and carbon isotopes analyses

About 0.4–1.4 g of olivine and 0.04–1.4 g of clinopyroxene crystals were hand-picked for noble gas and carbon isotopic measurements, then cleaned ultrasonically in 6.5 % HNO_3 before being rinsed with deionized water. The concentrations and isotopic compositions of noble gases (He, Ne, and Ar) and CO_2 in both (i) FI hosted in mineral separates from lavas/tephra/enclaves and (ii) fumaroles were analysed at the INGV, Sezione di Palermo isotopic laboratories, Italy. The gases hosted in mineral separates, were analysed by in vacuo single-step crushing at about 200 bars. This procedure minimizes the release of cosmogenic ^{3}He and radiogenic ^{4}He from the crystal matrix (Kurz, 1986), but it implies that bulk fluids are released, resulting in an average composition for the minerals (olivine, clinopyroxene) in each sample. Therefore, a contribution of gas inclusions within melt inclusions (i.e., shrinkage bubbles),

Table 1
List of the analysed samples. NG= Noble gases isotopes; C= carbon isotopes; R= Raman; M= Mineral chemistry. (*) Samples analysed in previous work (Lo Forte et al., 2023).

Sample name	Rock type	Rock composition	Eruption age	Analyses performed	Coordinates
Fog 20 (*)	Lava	Basanite	1799 C.E.	NG	14° 57′ 41.5″ N 24° 17′ 39.6″ W
Fog 23 (*)	Lava	Basanite	1664 C.E.	NG	15° 0′ 24.9″ N 24° 18′ 19.2″ W
Fog 24 (*)	Lava	Basanite	1852 C.E.	NG	15° 0′ 40.1″ N 24° 18′ 22.8″ W
Fog 27 (*)	Lava	Basanite	~60 ka	NG	14° 52′ 13.0″ N 24° 22′ 7.5″ W
Fog 28 (*)	Lava	/	~10 ka	NG	14° 58′ 11.8″ N 24° 20′ 59.5″ W
Fog 31 (*)	Lava	/	1951 C.E.	NG	14° 55′ 1.2″ N 24° 17′ 45.7″ W
Fog 33 (*)	Lava	Basanite	1400s-1800s	NG, C	14° 57′ 3.7″ N 24° 20′ 30.9″ W
Fog 43 (*)	Tephra	/	~10 ka	NG	15° 0′ 53.6″ N 24° 24′ 34.7″ W
FG1-A	Enclave	/	~10 ka	NG, C, R, M	14° 58′ 50.9″ N 24° 22′ 11.4″ W
FG2-A1	Enclave	/	1951 C.E.	NG, M	14° 58′ 50.0″ N 24° 21′ 20.3″ W
FG2-A3	Enclave	/	1951 C.E.	NG, R, M	14° 58′ 50.0″ N 24° 21′ 20.3″ W
FG3-A	Enclave	/	1400s-1800 s	NG, C, R, M	14° 57′ 6.10″ N 24° 20′ 33.45″ W
FG4-A	Enclave	/	~10 ka	NG, R, M	14° 58′ 14.1″ N 24° 22′ 05.4″ W
FG4-B	Enclave	/	~10 ka	NG, M	14° 58′ 14.1″ N 24° 22′ 05.4″ W
FG4-D	Enclave	/	~10 ka	NG, M	14° 58′ 14.1″ N 24° 22′ 05.4″ W
FG4-E	Enclave	/	~10 ka	NG, R, M	14° 58′ 14.1″ N 24° 22′ 05.4″ W
Pico do Fogo1	Fumarole	/	/	NG, C	14° 57′ 1.6″ N 24° 20′ 27.9″
Pico do Fogo 2	Fumarole	/	/	NG, C	14° 57′ 2.3″ N 24° 20′ 26.5″

as well as from FI, cannot be excluded.

3.2.1. *Isotope compositions of He, Ne, Ar, and CO_2 in fluid inclusions*

The selected crystals were divided into two aliquots: a first aliquot was used for noble gas isotopes measurement, while the second one was used to determine the concentration and isotope composition of CO_2. A first manometric quantification of CO_2 concentration in FI was performed during noble gas extraction. The noble gases were subsequently purified in an ultra-high-vacuum (10^{-9}–10^{-10} mbar) preparation system, where all species in the gas mixture, except for the noble gases, were removed under getters and cold fingers with active charcoal.

Helium isotopes (^{3}He and ^{4}He) and ^{20}Ne were measured separately using two different split-flight-tube mass spectrometers (Helix SFT, Thermo Scientific). ^{3}He/^{4}He ratios are expressed in units of R/Ra, where Ra represents the ^{3}He/^{4}He ratio of air, which is equal to 1.39×10^{-6} (Ozima and Podosek, 2002). The analytical uncertainty of the He-isotope ratio (1σ) was generally <1.6 %. The ^{20}Ne was corrected for isobaric interferences at *m/z* values of 20 ($^{40}Ar^{2+}$). The ^{36}Ar, ^{38}Ar, and ^{40}Ar were analysed using a multi-collector mass spectrometer (Argus, GVI) with an analytical uncertainty (1σ) of <0.5 %. In each analytical session, we analyzed at least one air standard for He, Ne, and Ar, which had been previously purified or stored in tanks. The analytical uncertainties (1σ) for the ^{3}He/^{4}He and ^{40}Ar/^{36}Ar ratios were <1 % and <0.06 %, respectively. The uncertainty in the elemental He, Ne, and Ar content determinations was <5 %, considering natural variability and the assumption of residual (not crushed) crystals for weight normalization of the number of moles of gas. Typical blanks for He, Ne, and Ar were $<10^{-15}$, $<10^{-16}$, and $<10^{-14}$ mol, respectively, that can be considered negligible respect to the amount of noble gases extracted from the crystals. Additional information regarding analytical procedures, adopted standards and their precision over time, can be found in Rizzo et al. (2018, 2021), and in Sandoval-Velasquez et al. (2021a, 2021b, 2023, 2024).

The ^{40}Ar was corrected for air contamination (^{40}Ar*) as follows:

$$^{40}Ar^* = {}^{40}Ar_{sample} - [{}^{36}Ar_{sample} \cdot ({}^{40}Ar/{}^{36}Ar)_{air}]$$

The ^{3}He/^{4}He ratio was corrected for atmospheric contamination (Rc/Ra) by utilizing the measured ^{4}He/^{20}Ne ratio, as follows:

$$Rc/Ra = ((R_M/Ra)(He/Ne)_M - (He/Ne)_A)/((He/Ne)_M - (He/Ne)_A)$$

where Rc stands for the air-corrected ^{3}He/^{4}He ratios, and subscripts M and A represent measured and atmospheric theoretical values, respectively.

Following the noble gas analysis, three aliquots with the highest CO_2 concentrations (olivines from the samples Fog33 and FG3-A, and clinopyroxene from the sample FG1A) were selected for determining the carbon isotopic composition of FI (^{13}C/^{12}C), which is reported as δ^{13}C in parts per mil (‰) relative to the Vienna Pee Dee Belemnite international standard (V-PDB). The samples for the carbon isotope analyses were extracted from a single-step crushing with an on-line glass trap freezed under liquid nitrogen and quantified using a glass line to prevent the adsorption and fractionation of CO_2 that can occur with powders and stainless-steel contact. We found agreement between the number of moles of CO_2 extracted and quantified in the glass line and those measured during noble gas extraction. After purification, the CO_2 was trapped in a glass sampler and transferred to the INGV-Palermo stable-isotope laboratory for IRMS measurements. Further details about the extraction and analytical protocol can be found in Rizzo et al. (2018, 2021), Sandoval-Velasquez et al. (2021a, 2021b, 2023, 2024) and

references therein. The $^{13}C/^{12}C$ ratio is expressed in delta notation ($\delta^{13}C$) as the difference in parts per mil relative to the V-PDB international standard. The analytical error, estimated as 1σ, was better than 0.3 ‰.

Noble gas and carbon isotope results are listed in Table S1 of the Supplementary Material S1.

3.2.2. Isotope compositions of He, Ne, Ar, and CO_2 in fumaroles

Fumarole gas samples were collected as "dry gas" in glass and stainless-steel bottles with two stopcocks, following the procedure reported in Rizzo et al. (2015). Major gas concentrations were measured by a gas chromatograph (Clarus 500, Perkin Elmer) equipped with a 30-meter column (inner diameter = 0.32 mm; Poraplot-Q), operated at a constant temperature of 50 °C using helium as the carrier gas, at the laboratory of INGV.

^3He, ^4He, and ^{20}Ne, as well as the $^4He/^{20}Ne$ ratios, were measured by introducing He and Ne separately into a split-flight tube mass spectrometer (GVI-Helix SFT, for He analysis) and a multi-collector mass spectrometer (Thermo-Helix MC plus, for Ne analysis) after standard purification procedures (Rizzo et al., 2016).

The carbon isotope composition of CO_2, expressed as $\delta^{13}C$ vs. V-PDB, was determined using a continuous-flow isotope-ratio mass spectrometer (Thermo Delta Plus XP, Finnigan) connected to a gas chromatograph (Trace GC) and interface (Thermo GC/C III, Finnigan). The standard deviation (SDs) for the $\delta^{13}C$ was <0.2 ‰.

Further details on the analytical procedure and adopted standards are the same reported in Rizzo et al. (2015, 2016, 2019). The chemical and isotopic compositions of dry gases are reported in Table S1 of Supplementary Material 1.

4. Results

The studied FI consist of pure CO_2. The CO_2 concentration in mafic enclaves ranges from 0.09 to $8.8{\cdot}10^{-8}$ mol/g in olivine crystals, and from 0.0008 mol/g to $6.7{\cdot}10^{-7}$ mol/g in clinopyroxene crystals. For comparison, in olivine crystals hosted in lavas and tephra, CO_2 concentrations span from 0.14 to $1.2{\cdot}10^{-8}$ mol/g. The CO_2 concentrations in the two fumaroles are >96 % vol. (Table S1 in the Supplementary Material S1).

The $\delta^{13}C$ isotope compositions of CO_2 in FI from crystals in mafic enclaves vary from −6.04 to −4.73 ‰. The most negative $\delta^{13}C$ value is obtained for FI in clinopyroxene crystals in sample FG1-A, while the most positive compositions are found in olivine crystals of sample FG3-A. The $\delta^{13}C$ of CO_2 in the two fumarolic samples are overall consistent with the FI results, and range from −5.1 to −4.7 ‰ for PF-2 and PF-1, respectively.

The $^3He/^4He$ ratios range from 7.35 to 8.18 Ra and from 7.86 to 8.44 Ra in olivine-hosted and clinopyroxene-hosted FI in mafic enclaves, respectively; from 7.14 to 8.25 Ra in olivine crystals from lava and tephra samples, and from 8.06 to 8.07 Ra in the fumaroles (Fig. 3).

In the mafic enclaves, the $^4He/^{20}Ne$ ratios vary between 167 and 746 in olivine-hosted FI, and between 99 and 2388 in clinopyroxene-hosted FI (Fig. 3). The $^4He/^{20}Ne$ ratios range from 10 to 468 for FI in crystals from lava and tephra samples, and from 37 to 104 in the fumaroles. The $^4He/^{20}Ne$ values, in both FI and fumaroles, are high enough that the correction for air contamination is insignificant for all the samples.

The $^{40}Ar/^{36}Ar$ values range from 339 to 1670 and from 315 to 1174 in FI from olivine and clinopyroxene crystals from mafic enclaves, and from 354 to 1758 in olivine crystals from lava and tephra samples. The observed $^{40}Ar/^{36}Ar$ ratios in the fumaroles PF-2 and PF-1 are from 324 to 397.

The $^4He/^{40}Ar^*$ ratios are 0.47–2.44 and 0.48–11.28 in FI from olivine and clinopyroxene crystals from mafic enclaves, 0.13–1.12 in olivine-hosted FI in lava and tephra, and 0.91–1.13 in fumaroles.

To simplify, in the discussion below we do not differentiate between lava and tephra samples and mafic enclaves due to their comparable isotopic compositions.

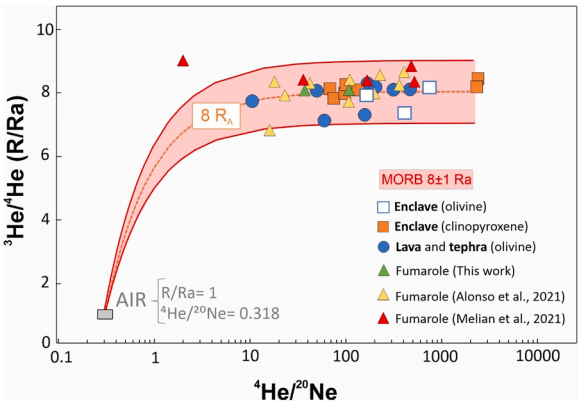

Fig. 3. $^3He/^4He$ expressed as R/Ra vs. $^4He/^{20}Ne$ data from Fogo. The binary mixing curves are between (i) air and a MORB-like (8 ± 1 Ra) magmatic endmember (8 ± 1). Endmembers values from Clarke et al. (1976) and Ozima and Podosek (2002) for the AIR and from Graham (2002) for MORB-like.

5. Discussion

5.1. Barometric estimations and Fogo storage system

The conditions of magmas storage underneath Fogo volcano have been established previously by using mineral barometers (Klügel et al., 2020), FI microthermometry (Hildner et al., 2011, 2012; Lo Forte et al., 2023), and melt inclusions geochemistry (DeVitre et al., 2023; Lo Forte et al., 2024) (Fig. 4a). Based on these results, a complex, magma storage system has been reconstructed (Fig. 4b), in which (1) magmas are initially stored in a deep reservoir at 773–1020 MPa (27–36 km depth); (2) an intermediate storage zone, constituted by distinct ponding levels, exists at 385–740 MPa pressure (~13–26 km depth); (3) upon pre-eruptive ascent, magmas eventually reside at 250–380 MPa pressure (~9–12 km depth) (Fig. 4a and b).

Our clinopyroxene barometric calculations for mafic enclaves (Table S3 in the Supplementary Material S1) confirm these results (Fig. 4a). Using the average temperatures of 1050 °C and 1130 °C for tephritic (Group Ia) and phonotephritic (Group Ib) melts (Klügel et al., 2020), respectively, clinopyroxene-based barometry (Eq. 32a; Putirka, 2008) yields equilibrium pressures of 536–737 (±130; ±standard deviation) MPa (18–26 km depth, using densities from the crustal model of Pim et al., 2008) for Group Ia and 336–464 (±144) MPa (12–16 km depth) for Group Ib (Fig. S2; 4a). These estimated pressures broadly overlap with those obtained previously by applying clinopyroxene barometry to Fogo lavas (e.g., Klügel et al., 2020) (Fig. 4a). We consider the distinct pressure ranges for the two groups of clinopyroxene crystals as statistically relevant, e.g., beyond uncertainty arising from experimental calibrations (Putirka et al., 2008). The shallow origin of these clinopyroxene crystal is also inferred from distinct elevated Ti/Al ratios (0.98 ± 0.74, on average for Group I vs. 0.26 ± 0.02 for Group II) that may suggest lower pressures of crystallization (Boudoire et al., 2019). The presence of sulphates in FI from this group (cf. Supplementary Material) likely reflects late-stage exsolution of SO_2-rich gas from magma and is therefore well consistent with a shallow magmatic environment.

The CO_2 densimetry of FI in clinopyroxene crystals broadly indicates lower pressures (<135 MPa) than inferred from clinopyroxene barometry (Table S2 of the Supplementary Material S1). Somewhat higher pressures (up to 350 MPa) are recorded by FI in olivine crystals (Fig. 4a), but still at the lower end of the clinopyroxene population. Previous works (Klügel et al., 2020; Boudoire et al., 2023; Lo Forte et al., 2023) documented a variety of post-entrapment processes affecting FI density (and hence the estimated entrapment pressure), including their

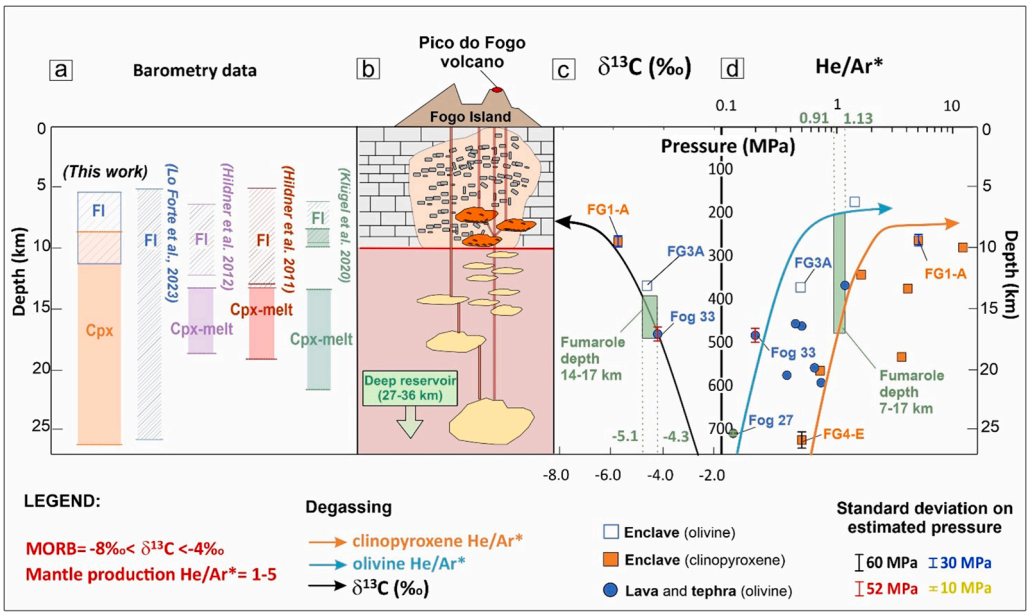

Fig. 4. a) Barometric data obtained from FI and clinopyroxene (cpx) analyses in our samples, compared with data from previous studies (Hildner et al., 2011, 2012; Klügel et al., 2020; Lo Forte et al., 2023). b) Schematic cross-section (not in scale) illustrating the internal structure of the Fogo magma system, adapted from Lo Forte et al. (2023), indicating the main magma storage zone (yellow magma pockets at 13–26 km depth) and the magma stagnation zone (orange magma pockets at 9–12 km depth). c) $\delta^{13}C$ values in FI vs. the corresponding pressure/depth. The modelled $\delta^{13}C$ compositions of the magmatic vapour phase (Eqs. (1) and 2) reproduce the observations related to a pressure-dependent isotopic fractionation due to magma degassing. See text for further details on modelling; d) He/Ar* ratios in FI vs. the corresponding pressure/depth. For pressure/depth, we use a combination clinopyroxene barometry (clinopyroxene crystals in mafic enclaves), FI densimetry (olivine crystals in mafic enclaves) and FI microthermometry (olivine crystals in lava and tephra). The diagram shows a broad He/Ar* ratio decrease with depressurization that is reproduced by an open-system degassing model (see text for explanations).

volumetric re-equilibration, and/or the precipitation of carbonates (observed by Raman; Fig. S3b in Supplementary Material). *Re*-equilibration of FI is known to be the strongest for clinopyroxenes (Klügel et al., 2000) as caused by plastic deformation of the host crystal during magma ascent and/or upon surface emplacement (for lavas; air-quenched tephra are less affected by this latter process). *Re*-equilibration is often substantial in FI entrapped in crystals from enclaves (Boudoire et al., 2023). However, we note that the highest estimated pressure (350 MPa for sample FG3-A) falls at the upper range of pressures (320–340 MPa) previously estimated by CO_2 densimetry in FI; the corresponding depth range (10.5–11.2 km) has been interpreted to reflect temporary magma storage near the Moho (Hildner et al., 2011, 2012; Lo Forte et al., 2023).

5.2. Magma degassing as revealed by C isotopes and noble gases

The isotopic compositions of CO_2 and ratios between noble gases (i.e., He/Ar*) in FI and fumaroles allow tracking magma degassing processes taking place during magma ascent from the mantle source, and eventually to back-calculate the composition of primary (undegassed) melt/gas (e.g., Boudoire et al., 2018 and references therein). This possibility is opened by the preferential partitioning of ^{13}C into a CO_2-rich vapour phase (relative to the coexisting melt), which leads to $\delta^{13}C$ of both melt and vapour to evolve towards increasingly lighter isotopic ratios upon increasing extents of degassing (Boudoire et al., 2018; Aubaud, 2022). If samples allow, this isotopic evolution can be traced (and modelled) using a suite of FI. Helium and argon, in view of their contrasting solubilities in silicate melts, are also extremely useful for reconstructing magmatic degassing. Argon is about 7–10 times less soluble than helium, and is hence enriched in the early (deeper) separated magmatic vapour phase (Iacono-Marziano et al., 2010 and references therein), causing the He/Ar* ratio to increase with increasing degassing extents (e.g., during magma decompression).

Fig. 4c and d highlight the $\delta^{13}C$ (CO_2) and He/Ar* signature of our FI samples as a function of the inferred FI entrapment pressure (see Section 5.1). We caution that our pressure estimates are based on a combination of different techniques, including clinopyroxene barometry (for clinopyroxenes in mafic enclaves), FI densimetry (for olivines in mafic enclaves) and FI microthermometry (for olivines in lavas and tephra), all of which are associated with relatively large uncertainties (especially clinopyroxene barometry, whose error can be as high as ±450 MPa). We hence consider possible, or even likely, that the distinct (broadly parallel) trends observed for olivine and clinopyroxene in the He/Ar* vs. pressure diagram (Fig. 4d) merely reflect a bias (a systematic offset) in the used barometric techniques. We find however that, independently on the mineral host, FI exhibit a marked pressure dependence, with the $\delta^{13}C$ (CO_2) progressively evolving toward lighter values, and He/Ar* manifestly increasing, with decreasing pressures (Fig. 4c,d). This pressure dependence can be used to model magmatic degassing. However, for the boundary conditions of the model we based on samples whose barometric estimation comes from FI techniques.

The FI carbon isotopic compositions range from −6.04 ‰ to −4.30 ‰ (Fig. 4c), within the MORB mantle range (−8‰ < $\delta^{13}C$ < −4 ‰; Sano and Marty, 1995). This MORB-like signature may be apparent and needs to be verified from models that consider isotopic fractionation during magma degassing. To quantitatively evaluate this process, we model the pressure-dependent evolution of both $\delta^{13}C$ and He/Ar* upon increasing extents of (decompression-driven) magmatic degassing, using the Fractional Equilibrium Degassing (FED) equations proposed by Macpherson and Mattey (1994) and applied by Boudoire et al. (2018) on a suite of FI from La Reunion Island:

$$\delta^{13}C_{(m)} = \delta^{13}C_{(m,i)} + (\Delta \cdot lnF) \quad \text{(Eq. 1)}$$

$$\delta^{13}C_{(v)} = \delta^{13}C_{(m)} + \Delta \quad \text{(Eq. 2)}$$

$$\frac{He}{Ar_{(g)}} = \frac{He}{Ar_{(g,\ i)}} \cdot \frac{K_{Ar}}{K_{He}} \cdot F^{\left(\frac{K_{Ar}}{K_{He}} - 1\right)} \quad \text{(Eq. 3)}$$

where F is residual fraction of gas remaining in the melt; in Eq. (1) and Eq. (2), $\delta^{13}C_{(m)}$, $\delta^{13}C_{(m,i)}$, and $\delta^{13}C_{(v)}$ are the carbon isotopes composition in the melt ($\delta^{13}C_{(m)}$) and in the vapour ($\delta^{13}C_{(v)}$) at each step of degassing path, and in the primary melt ($\delta^{13}C_{(m,i)}$); $\Delta = \delta^{13}C_{vapour} - \delta^{13}C_{melt}$ is the carbon isotope enrichment factor between vapour and melt, assumed at +2.74‰ as in other OIB-like melts (Boudoire et al., 2018). In Eq. (3), $\frac{He}{Ar(g)}$ *and* $\frac{He}{Ar(g,\ i)}$ are the ratios in gas (g) at respectively a given step (for a given F) of the degassing path, and in the early exsolved vapour (at the initial pressure); K_{Ar} and K_{He} are Ar and He (Henrian) solubility constants calculated from the model of Iacono-Marziano et al. (2010) based on the average composition of Fogo melts at about 730 MPa estimated for olivine Fog27 and clinopyroxene FG4-E and selected as starting conditions for the He/Ar* model (same approach used by Boudoire et al., 2018).

The $\delta^{13}C$-CO_2 degassing model is initialised using the following set of boundary conditions:

i) Sun and Dasgupta (2023) have shown that the primary melts at Cape Verde contain up to 9.1 wt.% of CO_2 and form by low degree of melting of a C-enriched mantle source;
ii) Eguchi and Dasgupta (2018) developed a CO_2 solubility model that, when applied to Fogo, converts the primary CO_2 content of 9.1 wt.% into a saturation pressure of ~2200 MPa (~77 km) (Fig. 5);
iii) The Lithosphere-Asthenosphere Boundary (LAB) below Cape Verde is estimated to range from 60 km (Liu et al., 2021) to 80 km (Lodge and Helffrich, 2006), with various studies placing the LAB within this range, suggesting depths of 65–70 km (Vinnik et al., 2012) and 70 km (Wilson et al., 2013).
iv) in FI from Fog33 olivines, we measured a $\delta^{13}C$ of −4.41 ‰ and estimated an average entrapment pressure of ~480 MPa (~17 km) (Figs. 4c and 5); based on the Eguchi and Dasgupta (2018) model, at this pressure the Fogo melt would contain ~0.78 wt.% CO_2 dissolved in the melt, fixing the residual fraction (F) at ~0.08 (i.e., ~92 % of the Fog33-type primary dissolved CO_2 is already lost due to magmatic degassing).
v) in our model, the magmatic vapour is then set to have a $\delta^{13}C$ (CO_2) of ~ −4.41 ‰ at $F = 0.08$, as measured in Fog33 olivines (Fig. 4c).

Using the boundary conditions above, we use Eqs. (1) and 2 to back-calculate the $\delta^{13}C$ pressure-dependent evolution in both gas and melt (Figs. 4c and 5). For a Fog33-type primary melt with 9.1 wt.% dissolved CO_2 at ~2200 MPa pressure (~77 km), we constrain a $\delta^{13}C$-CO_2 in the melt of −0.4 ‰, corresponding to a $\delta^{13}C$-CO_2 of the Fog33-type primary vapour of +2.3 ‰ (Fig. 5). Notably, we find our model results to be relatively insensitive to the sample selected for estimating F (see points iii) and iv) above): for example, if we were to initialise the model from the composition of the two other FI samples for which we have $\delta^{13}C$ data available (FG3-A olivines and FG1-A clinopyroxenes), we would obtain back-calculated primary melt $\delta^{13}C$ values of −0.4 ‰ and 0.2 ‰, very close to those obtained with Fog33 olivines (−0.4 ‰). We additionally note that estimated $\delta^{13}C$ values vary in a relatively narrow range (< ±1 ‰) when standard deviations in pressure estimates (± 52 MPa and ± 30 MPa for Fog 33 and FG1-A, respectively) are considered.

We compare the predicted pressure dependence of melt carbon concentrations from the model of Eguchi and Dasgupta (2018) with the model of Iacono-Marziano et al. (2012), a model commonly used for alkaline mafic compositions but calibrated at lower pressures (see Figure S4 in the Supplementary Material). We find that, for same CO_2 concentration in the melt, the model by Iacono-Marziano et al. (2012) returns a lower degassing pressure compared to that of Eguchi and Dasgupta (2018), with the two model outputs diverging more and more with increasing pressure (Figure S4). However, we find that even using the model of Iacono-Marziano et al. (2012) the $\delta^{13}C$ values of carbon dissolved in the primary melt (−0.84 ‰) and in the primary vapour (+1.90 ‰) remain isotopically heavy, and hence (as for the Eguchi and Dasgupta model) support a mantle source metasomatized by C-rich melts/fluids derived from a crustal component. We still consider the results obtained with the model of Eguchi and Dasgupta (2018) more

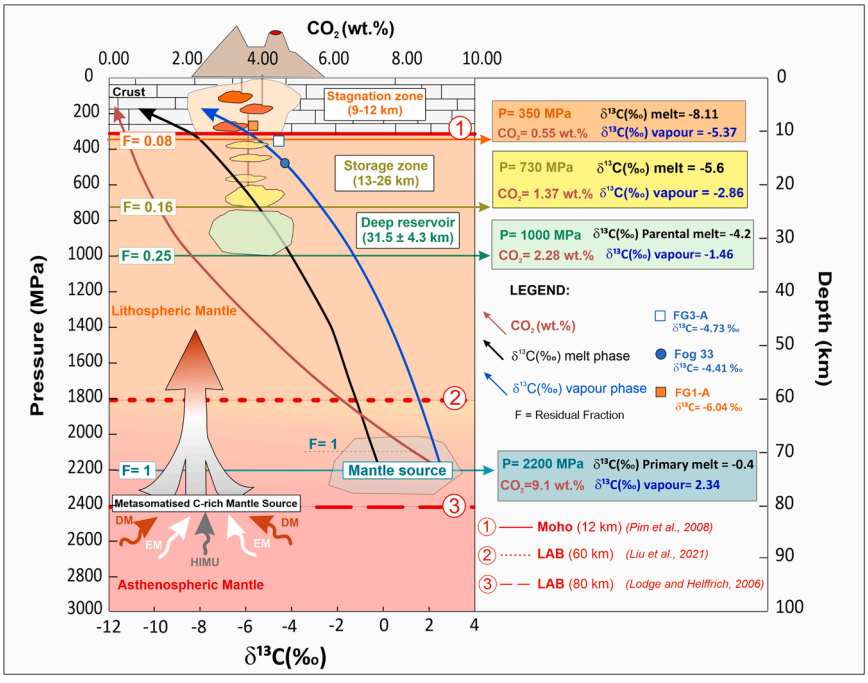

Fig. 5. Conceptual model for CO_2 degassing in the Fogo storage system, illustrating the pressure-dependent evolution of (i) dissolved CO_2 in the melt (red line), (ii) $\delta^{13}C$ in the melt phase (black line), and (iii) $\delta^{13}C$ in the vapour phase (blue line). The three curves are derived from degassing simulations. See text for description. The three different red lines (1,2,3) correspond to the Moho discontinuity (Pim et al., 2008) and to the Lithosphere-Asthenosphere Boundary (Liu et al., 2021; Lodge and Helffrich, 2006).

sound, as this model has been calibrated with experiments run at much higher pressures than those used by Iacono-Marziano et al. (2012) (<0.42 GPa).

Similarly, for the He/Ar* model, we constrain the boundary conditions considering the entrapment pressures (737 ± 60 and 720 ± 10 MPa) and He/Ar* ratios (0.48 ± 0.03 and 0.13 ± 0.01) of FI in FG4-E clinopyroxenes and Fog 27 olivines, respectively (Fig. 4d), the deepest trapped FI in our dataset. We remind that the barometric estimations in olivine and clinopyroxene samples were conducted using a combination of different techniques, each with its own set of uncertainties. Additionally, in the technique relying on FI, it's important to consider the possibility of resetting and re-equilibration of the FI at pressures lower than the initial fluid entrapment pressures. Hence, we cannot rule out the possibility of a slight bias in plotting the He/Ar* vs pressure data for the two mineral phases.

Based on this, we explore two possible paths of degassing to attempt a back-calculation of primary He/Ar* ratios. Based on the model by Eguchi and Dasgupta (2018), a pressure of ~730 MPa would imply a dissolved CO_2 content of ~1.4 wt.% and hence a F~0.15. Assuming the vapour phase to have a He/Ar* of ~0.5 and 0.1 at $F = 0.15$ (in FG4-E clinopyroxenes and Fog 27 olivines, respectively), we can use Eq. (3) to back-calculate the pressure-dependent evolution of the He/Ar* ratio upon degassing (Figs. 4d and 5). From this, we constrain a source He/Ar* ratio of 0.90–0.24 (Fig. 4d), which implies a variably depleted mantle with a He/Ar* lower than the U+Th/K production ratio assumed for the upper mantle (He/Ar = 1–5; Marty, 2012). The standard deviations associated with the FG4-E and Fog 27 estimated pressures convert into a relatively small He/Ar* ratio error (< ± 0.12).

The modelled pressure dependencies (Fig. 4b,c), if used in combination with Fogo fumarole compositions ($\delta^{13}C$ and He/Ar*), allow to infer the depth interval of the degassing magma that source the summit Fogo fumaroles. From this exercise, we propose the fumaroles are supplied by magmatic gas delivered by melts stored at ~13–17 km depth, in the intermediate storage zone located in the mantle (Fig. 4b,c).

5.3. Crustal carbon in the Cape Verde mantle source

Sun and Dasgupta (2023) reported that primary melts at Cape Verde may contain as high as 9 wt.% CO_2, converting into >400 ppm C in the mantle source (Lo Forte et al., 2024). One important corollary of this extremely high primary CO_2 content is that CO_2 saturation would be reached by magmas while deep in the mantle at ~2200 MPa (~77 km), according to the model of Eguchi and Dasgupta (2018). This depth aligns closely with the Lithosphere-Asthenosphere Boundary (LAB), which is estimated to range from 60 km (Liu et al., 2021) to 80 km (Lodge and Helffrich, 2006), with various studies placing the LAB within this range, suggesting depths of 65–70 km (Vinnik et al., 2012) and 70 km (Wilson et al., 2013). Consequently, even the deepest melts entrapped in olivine crystals as melt inclusions (at 896 ± 175 MPa, or 27–36 km), containing up to 2.3 wt.% dissolved CO_2 (DeVitre et al., 2023; Lo Forte et al., 2024), are extremely degassed ($F = 0.25$). Likewise, in view of our modelled $\delta^{13}C$ and He/Ar* pressure dependences (Figs. 4c,d and 5), magmatic vapours entrapped in FI (at pressures ≤740 MPa, or ≤25 km) or fumarole gases would be representative of "late-exsolved" magmatic vapours, whose isotopic compositions would in no way reflect that of primary melts, and of the mantle source. In their study on La Reunion Island, Boudoire et al. (2018) similarly found that gas entrapped in FI from local magmas located at mantle depths (~13 km) displays $\delta^{13}C$ of ~ −6 ‰ and He/Ar* of ~2. In this depth range, magmas have already lost ~90 % of their original (primary melt) dissolved CO_2 (inferred at up to 3.5 wt. %) and are therefore isotopically depleted in ^{13}C relative to their source (characterised at $\delta^{13}C$ ~ −0.8 ‰).

In our model for Fogo storage system (Fig. 5), we obtain primary $\delta^{13}C$ values for both dissolved C ($\delta^{13}C_{melt}$ of −0.4 ‰) and coexisting (early) vapour ($\delta^{13}C_{CO2}$ of 2.34 ‰) that are extremely more positive than recorded in the gas entrapped in FI and in fumarole gases. We caution that our calculations are based on a very limited dataset of only three samples; hence, also considering the large uncertainties in barometric estimation, a far larger dataset would therefore be required if more robust conclusions were to be reached. Yet, our calculations suggest that, if OIB magmas are as C-rich as recently suggested (Boudoire et al., 2018; Aiuppa et al., 2021; Burton et al., 2023; Sun and Dasgupta, 2023 and references therein, Van Gerve et al., 2024), then FI in magmatic products (e.g., lavas, tephra, crustal/mantle cumulates, and submarine glasses) and/or in fumarole gases may hardly record the C isotopic signature at source (Boudoire et al., 2018; Aubaud et al., 2022; Sandoval Velasquez et al., 2023; this work), unless carefully modelled for degassing. FI in mantle xenoliths should be prioritised for this purpose, as they are generally brought to the surface from high depths in the mantle with no or little degassing (e.g., Haggerty and Sautter, 1990). In this context, Fig. 6 highlights that our modelled primary melt/gas $\delta^{13}C$ signatures (−0.4 ‰/+2.23 ‰) match closely those inferred for El Hierro ($\delta^{13}C = -0.96$‰), La Palma ($\delta^{13}C = -1.70$ ‰) and Lanzarote ($\delta^{13}C = -0.80$ ‰) mantle sources from nearby Canary Island OIB, as determined by analysing FI in mantle xenoliths (-2.38 ‰ < $\delta^{13}C$ < 0.96 ‰, Sandoval-Velasquez et al., 2021a, 2023; 2024).

A ^{13}C-enriched signature for Fogo primary melts, if confirmed by future studies, would provide decisive clues for the existence of a metasomatized (C-enriched) mantle source underneath Cape Verde, as recently indicated by melt inclusions studies (e.g., De Vitre et al., 2023; Lo Forte et al., 2024), magma petrology (Sun and Dasgupta, 2023), mantle xenoliths (Bonadiman et al., 2005), and by the rare carbonatites (Foeken et al., 2007). The mantle metasomatism involving carbonatitic to carbonated-silicate melts within the Cape Verde archipelago, may potentially reflect the recycling of old, deeply subducted (e.g., Hoernle et al., 2002) crustal materials ($\delta^{13}C \geq -1$ ‰) into the local deep mantle (e.g., Dorfman et al., 2018 and references therein). The HIMU affinity of

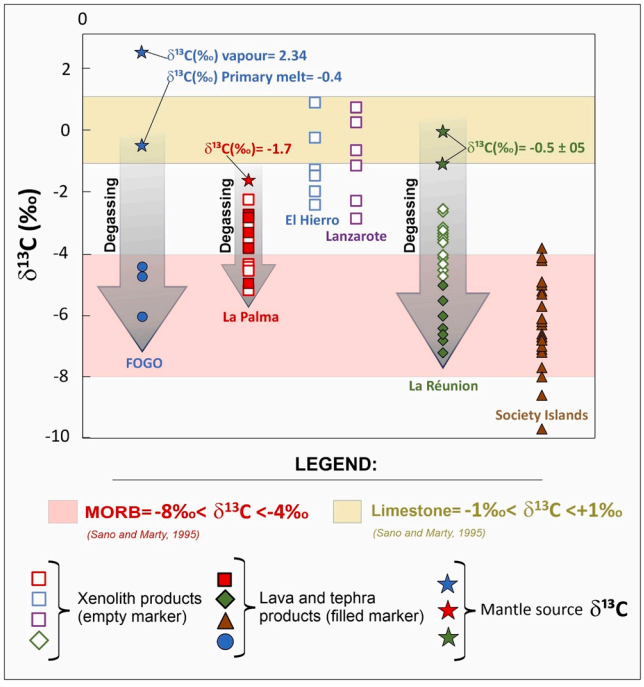

Fig. 6. $\delta^{13}C$ range of values for: Fogo, in Cape Verde archipelago; El Hierro, Lanzarote, and La Palma, in the Canary Islands (Sandoval et al., 2021a, 2023); Piton de la Fournaise, in La Réunion Island (Boudoire et al., 2018); Society Islands (Aubaud et al., 2006). The samples include ultramafic xenoliths (e.g., El Hierro, Lanzarote, La Palma, La Réunion), lavas and tephra (La Palma, La Réunion, Fogo), and submarine lavas (Society Islands). The black arrows indicate the degassing path from the primary melts/mantle source (estimated for Fogo, La Palma, and La Réunion). It is worth of note that many samples from the selected areas fall (apparently) in the MORB range.

many recent lavas at Fogo, and in the Cape Verde archipelago in general (Mata et al., 2017), would well be consistent with the presence of a recycled crustal component (e.g., old altered oceanic crust and oceanic lithosphere) in the local mantle. Alternatively, the presence of relicts of subcontinental mantle lithosphere related to the opening of the Central Atlantic Ocean should be considered (Bonadiman et al., 2005). However, this model needs geodynamic constraints.

Recent FI measurements (Fig. 6) in mantle xenoliths bring increasing evidence for the mantle source(s) of continental rift and OIB volcanism (e.g., Rizzo et al., 2018; Sandoval-Velasquez et al., 2021a, 2021b, 2023; Halldorsson et al., 2022; Remigi et al., 2023) to be more ^{13}C-rich than previously thought (Deines, 2002); in light of this, a crustal carbon component in the local mantle could explain this evidence. If so, some of the light-carbon OIB signatures observed so far (e.g., Society Islands; Fig. 6) may result from the entrapment in lavas/glasses of volatiles representative of late stages of magmatic degassing, containing a

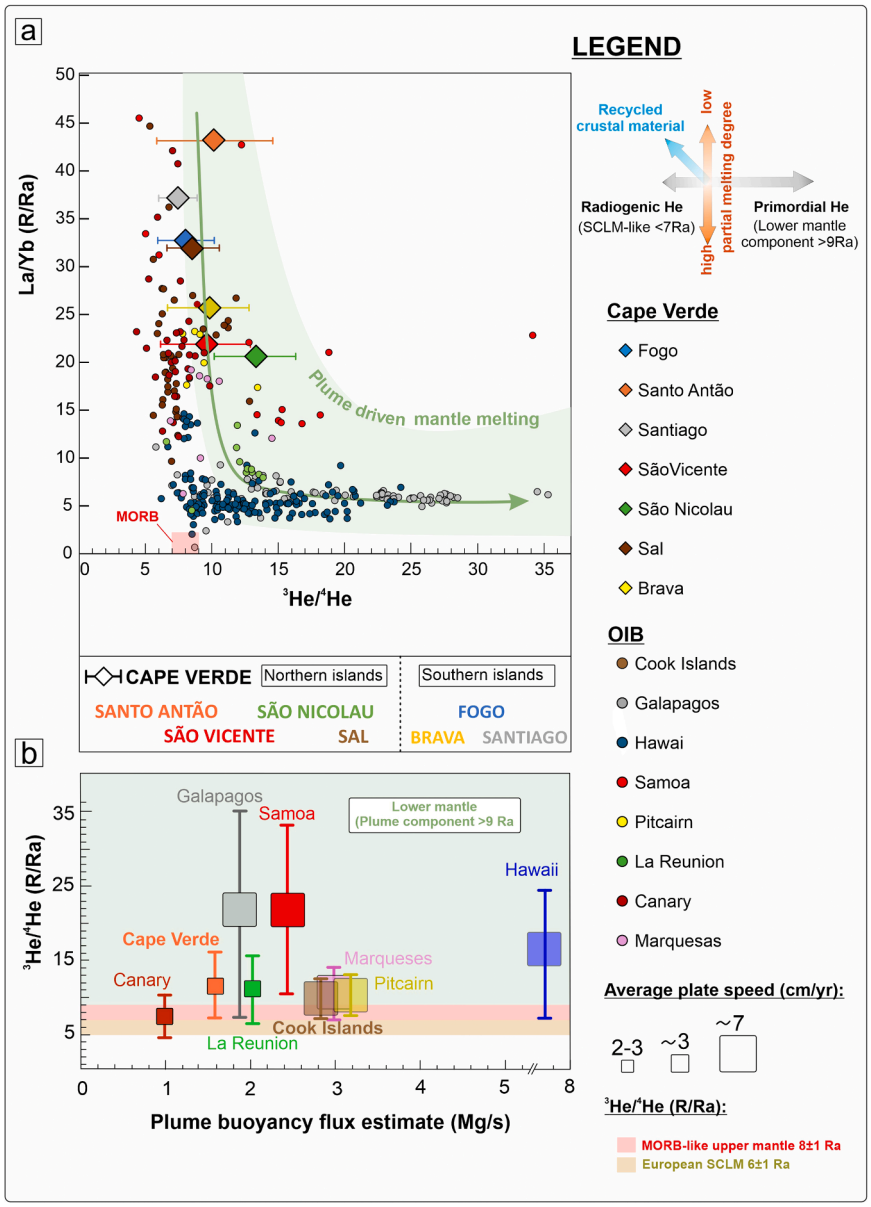

Fig. 7. (a) La/Yb ratio vs. ^{3}He/^{4}He ratio for Cape Verde (after the data filtering, see Section 1, Fig. 1, for further details) and other OIB localities. The He isotope compositions of Cape Verde are from this work and literature data (e.g., Christensen et al., 2001, Doucelance et al., 2003), whereas La/Yb and ^{3}He/^{4}He data for other islands are sourced from literature, as detailed in the Supplementary Material S3. The symbol (diamond for each Cape Verde island) indicates the mean ^{3}He/^{4}He value, whereas the bars represent the entire range of values for each Cape Verde islands. (b) Plume buoyancy flux vs. ^{3}He/^{4}He ratios vs. average plate speed in OIB localities. OIB, such as Cape Verde (^{3}He/^{4}He = 7–16 Ra, plume buoyancy flux 1.6 Mg/s, and average plate speed ~3 cm/yr) and the Canary Islands (^{3}He/^{4}He = 5–10 Ra, plume buoyancy flux 1.0 Mg/s, and average plate speed~ 3 cm/yr), are the lower end-members of the model. In contrast, OIB locations such as Galapagos and Hawaii, characterized by high ^{3}He/^{4}He values (up to 35 Ra), moderate to high plume buoyancy flux (~2 Mg/s for Galapagos and~ 8.0 Mg/s for Hawaii), and high average plate speed (~ 7 cm/yr), represent the upper end-members of the model. Intermediate OIB localities, such as La Réunion, Marquesas, Pitcairn, and the Cook Islands, fall within the ranges between these end-members. La Réunion exhibits ^{3}He/^{4}He ratios ranging from~ 7 to~ 16 Ra, plume buoyancy flux of 2 Mg/s, and an average plate speed of~ 3 cm/yr. Marquesas shows ^{3}He/^{4}He ratios from ~7 to~14 Ra, a plume buoyancy flux of 3.3 Mg/s, and an average plate speed of ~7 cm/yr. Pitcairn exhibits ^{3}He/^{4}He ratios from ~8 to~ 13 Ra, a plume buoyancy flux of 3.3 Mg/s, and an average plate speed of~7 cm/yr. Cook Islands demonstrate ^{3}He/^{4}He ratios from~ 6 to ~11 Ra, a plume buoyancy flux of 3.3 Mg/s, and an average plate speed of ~7 cm/yr. Plume buoyancy flux data and average plate speeds are from Hoggard et al. (2020) and references therein.

fractionated ^{13}C-depleted residual carbon fraction, rather than mantle rock specimens.

5.4. Regional He isotope trends

Helium isotopes for Fogo point to a relatively uniform MORB-type mantle with $^{3}He/^{4}He$ ~8 ± 1 Ra (Figs. 2 and 3), as inferred previously (e.g., Doucelance et al., 2003). We cannot exclude that this isotopic signature results from a mixing between a lower mantle component with higher than MORB $^{3}He/^{4}He$ values and crustal-derived fluids (from recycled crustal material bearing U and Th) with more radiogenic ratios.

A question that remains open is what controls the regional variability of $^{3}He/^{4}He$ compositions, and specifically how the Fogo MORB-like signature can be reconciled with a regional context where a ^{3}He-richer component (R_c/R_a >9) has been identified both in northern and southern islands (Figs. 2 and 7a) (Christensen et al., 2001; Doucelance et al., 2003; Day et al., 2022). Fig. 7a explores the relationship between the $^{3}He/^{4}He$ compositions of the different Cape Verde archipelago islands and their averaged bulk rock La/Yb ratios. We use this trace element proxy as a marker of the extent of partial melting of the source mantle (with high ratios corresponding to low degrees of melting; Stracke and Bourdon, 2009), but we yet acknowledge that slab fluids formed by melting/dehydration of subducted crustal materials are high in La/Yb (Kessel et al., 2005). Hence, high La/Yb in OIB is considered to reflect a combination of low degrees of melting and mantle metasomatism by recycled crustal materials. The La/Yb ratio can additionally be modified by fractional crystallization, but to mitigate against this effect we select samples with MgO >8.00 wt.%. Nevertheless, we note that even more evolved (MgO-poorer) samples would exhibit a similar range of La/Yb ratios. Data for a few other OIBs (e.g., Canary, Cook Islands, Hawaii, Galapagos, La Réunion, Marquesas, Pitcairn, Samoa, and the Society Islands) are also shown.

The oceanic island dataset illustrated in Fig. 7a shows an inverse correlation, wherein La/Yb decreases with increasing $^{3}He/^{4}He$ ratios. At $^{3}He/^{4}He$ signatures >9 Ra, this tendency is explained by an increasing degree of mantle melting (lower La/Yb) caused by ascending mantle plumes, which are characterised by their primordial ^{3}He-rich, lower mantle signatures. The large spread of compositions seen at many of such OIB localities (see the wide range of $^{3}He/^{4}He$ at Hawaii and Galapagos at relatively invariant - and low - La/Yb) imply a high level of source heterogeneity. In contract, Ocean islands exhibiting high La/Yb ratios are typically found to exhibit MORB or below-MORB He signatures, as represented by the Canaries, Cook Islands, and Fogo and Santiago, in the Cape Verde archipelago. In addition to indicating low degrees of melting, these MORB and especially below MORB compositions (where existent), when/if associated with high La/Yb ratios, reflect a mantle source where recycled crustal materials participate in the melting process, as often invoked for the eastern Canaries (Sandoval-Velasquez et al., 2021a, 2023; Day et al., 2022). At Fogo, this is well in agreement with our carbon isotope results above. Finally, Santo Antão, with its high La/Yb but higher than MORB (>9 Ra) $^{3}He/^{4}He$ signatures, is with São Nicolau the only Cape Verde OIB locality with a more evident lower mantle He contribution.

5.5. Implications for global OIB geodynamics

Recent studies of global OIBs (e.g., Jackson et al., 2017a,b; Day et al., 2022) have shown that higher than MORB $^{3}He/^{4}He$ (>9 Ra) - indicative of a lower mantle component - are systematically associated with low-velocity mantle regions related to ascending hot plumes. Fig. 7b illustrates the global OIB relationship between $^{3}He/^{4}He$, plume buoyancy flux, and plate speed, which we have updated and implemented from previous study (Day et al., 2022) using a refined Cape Verde archipelago-average. This is obtained by considering our Fogo results and the quality check/filtering of literature data discussed above (Figs. 1,2). The plume buoyancy fluxes (Hoggard et al., 2020) are inferred based on a volumetric approach, which considers (i) the density of the asthenospheric mantle, (ii) the density of displaced surface fluid, (iii) the volume of the swell, and (iv) a characteristic timescale of buoyancy loss.

The diagram corroborates previous evidences of Day et al. (2022) for the existence of a positive dependency between plates speed and OIB $^{3}He/^{4}He$ signatures, and suggests that OIB localities such as the Cape Verde and Canary Islands, which are thought to be associated with relatively low plume buoyancy fluxes (1–1.6 Mg/s, Hoggard et al., 2020) and low plates speed, are systematically characterised by more radiogenic $^{3}He/^{4}He$ ratios than those recorded at more buoyant plumes locations (e.g., Hawaii, Galapagos, Samoa). This relationship agrees with the hypothesis that (i) hot plumes are the source of OIB with high-$^{3}He/^{4}He$ ratios (Jackson et al., 2017a,b) and (ii) the plume buoyancy flux is higher in correspondence with faster moving plates (Hoggard et al., 2020). One of the factors that directly influences the plume buoyancy flux, and thus upwelling, is the density of the variably depleted mantle source, which decreases with increasing melt extraction (Schutt and Lesher, 2006). Thus, OIB with high degrees of melt extraction, such as Hawaii, Galapagos, and Samoa, also exhibit a high plume buoyancy flux (Fig. 7a,b).

The dichotomy between high (Hawaii, Galapagos) and low mantle flux (Cape Verde and Canary) OIB extends to the conditions of magma supply and storage. Indeed, recent barometric estimates indicate that magmas storage conditions at OIB vary from shallow-crustal (e.g., Kilauea, Hawaii) to deep-crust and/or upper mantle (e.g., Cape Verde and Canary Islands; La Réunion Island), mimicking a contrast in magma supply rate (3–4 m^3/s at Kilauea vs. 0.06 m^3/s at Fogo; see Boudoire et al., 2018; Lo Forte et al., 2023 and references therein). Taken together, this evidence suggests that magma storage is consistently shallower in magmatic systems above high buoyancy flux plumes coupled to high plates speed than in off-axis systems, or above low buoyancy flux plumes coupled to low plates speed. Thus, magma supply from the underlying mantle source coupled to the $^{3}He/^{4}He$ signature represents a first-order control on the depth of magma storage beneath ocean island volcanoes (e.g., Gleeson et al., 2021).

6. Conclusions

We present the first carbon isotopic measurements and new noble gas (He-Ne-Ar) data in FI hosted in olivine and clinopyroxene crystals from mafic enclaves, lavas, tephra and in volcanic gas samples from Fogo, the most active volcano of the Cape Verde archipelago (eastern Atlantic). The main findings can be summarized as follows:

- He isotopic systematics in our samples (mafic enclaves, lava, tephra, and fumarole) confirm a MORB-like upper mantle signature (R_c/R_a=7.14–8.44) for the lithospheric mantle beneath Fogo, consistent with the $^{3}He/^{4}He$ signatures previously reported for fumarole (e.g., Melian et al., 2021; Alonso et al., 2021) and FI (e.g., Christensen et al., 2001; Doucelance et al., 2003).
- The carbon isotopic ratio ($\delta^{13}C$ vs. PDB) of CO_2 in FI and fumaroles range from −6.04 to −4.41 ‰, consistent with $\delta^{13}C$ values previously reported for fumarole (Melian et al., 2021; Alonso et al., 2021). This variability reflects isotopic fractionation due to high extents of magma degassing (~75–94 %) at shallow depths in the Fogo storage system. Systematic variations of $\delta^{13}C$ and He/Ar* coupled with FI entrapment pressure (as estimated from a combination of host mineral barometers and FI densimetry/microthermometry) allow us to develop a model for volatile degassing in the local storage system. From this model, we predict a crustal signature for carbon ($\delta^{13}C$ of ~ −0.4 ‰) in primary melts formed by upper mantle melting at ~2200 MPa (~77 km) and a source He/Ar* ratio of 0.90–0.24 (Fig. 4d) lower than the expected production ratio assumed for the upper mantle, which we interpret as indicative of a variably depleted

mantle metasomatized by melts/fluids enriched in a crustal carbon component.

- A ^{13}C-enriched signature for Fogo primary melts, similarly to what recently observed for Canary Islands (Sandoval-Velasquez et al., 2021a, 2023), may potentially reflect the presence of crustal materials ($\delta^{13}C \geq -1$ ‰) into the deep mantle beneath Cape Verde, as suggested by high CO_2 contents in primary melts (e.g., Dorfman et al., 2018 and references therein). This could imply that OIB volcanism is more ^{13}C-rich than previously thought (Deines, 2002), suggesting a recurrent crustal carbon component, such as carbonates, in the mantle (Hammouda et al., 2021).
- A careful review of existing $^{3}He/^{4}He$ literature in Cape Verde shows that He isotopes in OIB scale inversely with La/Yb ratio and, hence, with magma production rates in the mantle source. In detail, in Cape Verde the lower mantle component ($^{3}He/^{4}He$ ratio > 9 Ra) is evident in regions where high degrees of mantle melts prevail (i.e., relative low La/Yb ratio), with the island of Santo Antão exhibiting high $^{3}He/^{4}He$ (> 9 Ra) and the highest La/Yb ratio in the archipelago, being the only exception. Instead, in OIB plume-like environments (e.g., Marquesas, Pitcairn, Society Islands, Samoa, and Reunion), the lower mantle component is driven by the amplitude of the lower mantle component rather than to different degrees of partial melting. The MORB-like $^{3}He/^{4}He$ signature at Fogo reflects a combination of (i) low to medium magma productivity, (ii) relatively low plume buoyancy flux (~1.1 Mg/s), and (iii) slow average speed (~3 cm/yr) of the overlying plate.
- Ultimately, we propose that the dichotomy between high mantle flux (e.g., Hawaii, Galapagos) and low mantle flux (e.g., Cape Verde and Canary) OIB extends to the conditions of magma supply and storage.

CRediT authorship contribution statement

Francesco Maria Lo Forte: Writing – review & editing, Writing – original draft, Software, Methodology, Investigation, Data curation, Conceptualization. **Guillaume Boudoire:** Writing – review & editing, Writing – original draft, Software, Methodology, Investigation, Formal analysis, Data curation, Conceptualization. **Maria Luce Frezzotti:** Visualization, Validation, Supervision, Project administration, Methodology, Investigation, Funding acquisition, Conceptualization. **Silvio Giuseppe Rotolo:** Writing – original draft, Visualization, Validation, Data curation. **Andres Sandoval-Velasquez:** Visualization, Validation, Methodology, Investigation, Formal analysis, Data curation, Conceptualization. **Fátima Viveiros:** Visualization, Validation, Supervision, Conceptualization. **Vittorio Zanon:** Writing – original draft, Visualization, Validation, Methodology, Funding acquisition, Data curation, Conceptualization. **Alessandro Aiuppa:** Writing – review & editing, Writing – original draft, Visualization, Validation, Supervision, Project administration, Investigation, Funding acquisition, Formal analysis. **Andrea Luca Rizzo:** Writing – review & editing, Writing – original draft, Visualization, Validation, Supervision, Methodology, Investigation, Formal analysis, Data curation, Conceptualization.

Declaration of competing interest

The authors declare that they have no known competing financial interests or personal relationships that could have appeared to influence the work reported in this paper.

Data availability

Data will be made available on request.

Acknowledgements

This research was funded by the Italian Minister (PRIN2022HA8XCS), by the Fundação para a Ciência e Tecnologia (FCT), Portugal, through project MAGAT project (Ref. CIRCNA/OCT/2016/2019), and by the RETURN Extended Partnership and received funding from the European Union Next-GenerationEU (National Recovery and Resilience Plan – NRRP, Mission 4, Component 2, Investment 1.3 – D.D. 1243 2/8/2022, PE0000005).

We thank Mariano Tantillo and Mariagrazia Misseri for helping during the isotope analysis of noble and in the CO_2 extraction from minerals. Igor Oliveri and Giorgio Capasso are also acknowledged for the isotope analysis of carbon of CO_2 performed in the stable isotope laboratory of INGV-Palermo. Dr. Virginia Valenti is acknowledged for her invaluable assistance during the sampling fieldwork at Fogo and handpicking in the laboratory of the University of Milano-Bicocca. The authors wish to acknowledge constructive comments from the Editor (Fang-Zhen Teng), Mark Kurz, and one anonymous reviewer.

Supplementary materials

Supplementary material associated with this article can be found, in the online version, at doi:10.1016/j.epsl.2024.118930.

References

Aiuppa, A., Bitetto, M., Rizzo, A.L., Viveiros, F., Allard, P., Frezzotti, M.L., Zanon, V., 2020. The fumarolic CO_2 output from Pico do Fogo Volcano (Cape Verde). Ital. J. Geosci. 139 (3), 325–340. https://doi.org/10.3301/IJG.2020.03.

Aiuppa, A., Casetta, F., Coltorti, M., Stagno, V., Tamburello, G., 2021. Carbon concentration increases with depth of melting in Earth's upper mantle. Nat. Geosci. 14, 697–703. https://doi.org/10.1038/s41561-021-00797-y.

Alonso, M., Pérez, N.M., Padrón, E., Hernández, P.A., Melián, G.V., Sumino, H., Padilla, G.D., Barrancos, J., Rodríguez, F., Dionis, S., Asensio-Ramos, M., Amonte, C., Silva, S., Pereira, J.M., 2021. Changes in the thermal energy and the diffuse ^{3}He and ^{4}He degassing prior to the 2014–2015 eruption of Pico do Fogo volcano, Cape Verde. J. Volcanol. Geother. Res. 416, 107271 https://doi.org/10.1016/j.jvolgeores.2021.107271.

Aubaud, C., 2022. Carbon stable isotope constraints on CO_2 degassing models of ridge, hotspot and arc magmas. Chem. Geol. 605, 120962 https://doi.org/10.1016/j.epsl.2023.118307.

Aubaud, C., Pineau, F., Hékinian, R., Javoy, M., 2006. Carbon and hydrogen isotope constraints on degassing of CO_2 and H_2O in submarine lavas from the Pitcairn hotspot (South Pacific). Geophys. Res. Lett. 33, L02308. https://doi.org/10.1029/2005GL024907.

Barker, A.K., Magnusson, E., Troll, V.R., Harris, C., Mattsson, H.B., Holm, P.M., et al., 2023. Disequilibrium in historic volcanic rocks from Fogo, Cape Verde: traces of carbonatite metasomatism of recycled ocean crust. Lith 456-57, 107328. https://doi.org/10.1016/j.jvolgeores.2023.107996.

Bonadiman, C., Beccaluva, L., Coltorti, M., Siena, F., 2005. Kimberlite-like metasomatism and 'garnet signature' in spinel-peridotite xenoliths from sal, Cape Verde archipelago: relics of a subcontinental mantle domain within the atlantic oceanic lithosphere? J. Petrol. 46, 2465–2493. https://doi.org/10.1093/petrology/egi061.

Boudoire, G., Brugier, Y.-A., Di Muro, A., Wörner, G., Arienzo, I., Metrich, N., Zanon, V., Braukmüller, N., Kronz, A., Le Moigne, Y., Michon, L., 2019. Eruptive activity on the Western Flank of Piton de la Fournaise (La Réunion Island, Indian Ocean): insights on magma transfer, storage and evolution at an Oceanic Volcanic Island. J. Petrol. 60, 1717–1752. https://doi.org/10.1093/petrology/egz045.

Boudoire, G., Pasdeloup, G., Schiavi, F., Cluzel, N., Rafflin, V., Grassa …, F., Rizzo, A.L., 2023. Magma storage and degassing beneath the youngest volcanoes of the Massif Central (France): lessons for the monitoring of a dormant volcanic province. Chem. Geol. 121603 https://doi.org/10.1016/j.chemgeo.2023.121603.

Boudoire, G., Rizzo, A.L., Arienzo, I., Di Muro, A., 2020. Paroxysmal eruptions tracked by variations of helium isotopes: inferences from Piton de la Fournaise (La Réunion island). Sci. Rep. 10, 9809. https://doi.org/10.1038/s41598-020-66260-x.

Boudoire, G., Rizzo, A.L., Di Muro, A., Grassa, F., Liuzzo, M., 2018. Extensive CO_2 degassing in the upper mantle beneath oceanic basaltic volcanoes: first insights from Piton de la Fournaise volcano (La Réunion Island). Geochim. Cosmochim. Acta 235, 376–401. https://doi.org/10.1016/j.gca.2018.06.004.

Carvalho, J., Silveira, G., Kiselev, S., Custódio, S., Ramalho, R.S., Stutzmann, E., Schimmel, M., 2022. Crustal and uppermost mantle structure of Cape Verde from ambient noise tomography. Geophys. J. Int. 231, 1421–1433. https://doi.org/10.1093/gji/ggac254.

Christensen, B.P., Holm, P.M., Jambon, A., Wilson, J.R., 2001. Helium, argon and lead isotopic composition of volcanics from Santo Antão and Fogo, Cape Verde Islands. Chem. Geol. 178, 127–142. https://doi.org/10.1016/S0009-2541(01)00261-3.

Clarke, W.B., Jenkins, W.J., Top, Z., 1976. Determination of tritium by mass spectrometric measurement of 3He. Int. J. Appl. Radiat. Isot. 27, 515–522. https://doi.org/10.1016/0020-708X(76)90082-X.

Dasgupta, R., 2018. Volatile-bearing partial melts beneath oceans and continents–where, how much, and of what compositions? Am. J. Sci. 318 (1), 141–165. https://doi.org/10.2475/01.2018.06.

Day, S.J., Heleno da Silva, S.I.N., Fonseca, J.F.B.D., 1999. A past giant lateral collapse and present-day flank instability of Fogo, Cape Verde islands. J. Volcanol. and Geother. Res. 94, 191–218. https://doi.org/10.1016/S0377-0273(99)00103-1.

Day, J.M.D., Jones, T.D., Nicklas, R.W., 2022. Mantle sources of ocean islands basalts revealed from noble gas isotope systematics. Chem. Geol. 587, 120626 https://doi.org/10.1016/j.chemgeo.2021.120626.

Deines, P., 2002. The carbon isotope geochemistry of mantle xenoliths. Earth-Sci. Rev. 58, 247–278. https://doi.org/10.1016/S0012-8252(02)00064-8.

DeVitre, C.L., Gazel, E., Ramalho, R.S., Venugopal, S., Steele-MacInnis, M., Hua, J., Allison, C.M., Moore, L.R., Carracedo, J.C., Monteleone, B., 2023. Oceanic intraplate explosive eruptions fed directly from the mantle. Proc. Natl. Acad. Sci. 120 (33), e2302093120 https://doi.org/10.1073/pnas.2302093120.

Dorfman, S.M., Badro, J., Nabiei, F., Prakapenka, V.B., Cantoni, M., Gillet, P., 2018. Carbonate stability in the reduced lower mantle. Earth Planet. Sci. Lett. 489, 84–91. https://doi.org/10.1016/j.epsl.2018.02.035.

Doucelance, R., Escrig, S., Moreira, M., Gariépy, C., Kurz, M.D., 2003. Pb-Sr-He isotope and trace element geochemistry of the Cape Verde Archipelago. Geochim. Cosmochim. Acta 67, 3717–3733. https://doi.org/10.1016/S0016-7037(03)00161-3.

Dunai, T.J., Porcelli, D., 2002. Storage and transport of noble gases in the subcontinental lithosphere. Rev. Mineral. Geochem. 47, 371–409. https://doi.org/10.2138/rmg.2002.47.10.

Eguchi, J., Dasgupta, R., 2018. A CO_2 solubility model for silicate melts from fluid saturation to graphite or diamond saturation. Chem. Geol. 487, 23–38. https://doi.org/10.1016/j.chemgeo.2018.04.012.

Frezzotti, M.L., Peccerillo, A., 2004. Fluid inclusion and petrological studies elucidate reconstruction of magma conduits. Trans. Am. Geophys. Union 85 (16), 157–163. https://doi.org/10.1029/2004EO160001.

Frezzotti, M.L., Burke, E.A.J., De Vivo, B., Stefanini, B., Villa, I.M., 1992. Mantle fluids in pyroxenite nodules from Salt Lake Crater (Oahu, Hawaii). Eur. J. Min. 4, 1137–1153. https://doi.org/10.1127/ejm/4/5/1137.

Frezzotti, M.L., Andersen, T., Neumann, E.R., Simonsen, S.L., 2002. Carbonatite melt-CO_2 fluid inclusions inmantle xenoliths from Tenerife, Canary Islands: a story of trapping, immiscibility and fluid–rock interaction in the upper mantle. Lithos 64, 77–96. https://doi.org/10.1016/S0024-4937(02)00178-0.

Gautheron, C., Moreira, M., Allègre, C., 2005. He, Ne and Ar composition of the European lithospheric mantle. Chem. Geol. 217, 97–112. https://doi.org/10.1016/j.chemgeo.2004.12.009.

Gerlach, D.C., Cliff, R.A., Davies, G.R., Norry, M., Hodgson, N., 1988. Magma sources of the Cape Verdes archipelago: isotopic and trace element constraints. Geochim. Cosmochim. Acta 52, 2979–2992. https://doi.org/10.1016/0016-7037(88)90162-7.

Gleeson, M.L.M., Gibson, S.A., Stock, M.J., 2021. Upper mantle mush zones beneath low melt flux Ocean Island volcanoes: insights from Isla Floreana, Galápagos. J. Petrol. 61, egaa094. https://doi.org/10.1093/petrology/egaa094.

Graham, D.W., 2002. Noble gas isotope geochemistry of mid-ocean ridge and ocean island basalts: characterization of mantle source reservoirs. Rev. Min. Geochem. 47, 247–317. https://doi.org/10.2138/rmg.2002.47.8.

Hammouda, T., Manthilake, G., Goncalves, P., Chantel, J., Guignard, J., Crichton, W., et al., 2021. Is there a global carbonate layer in the oceanic mantle? Geophys. Res. Lett. 48 (2), e2020GL089752 https://doi.org/10.1029/2020GL089752.

Haggerty, S.E., Sautter, V., 1990. Ultradeep (greater than 300 kms), ultramafic upper mantle xenoliths. Science 248, 993–996. https://doi.org/10.1126/science.248.4958.99.

Hildner, E., Klügel, A., Hansteen, T.H., 2012. Barometry of lavas from the 1951 eruption of Fogo, Cape Verde islands: implications for historic and prehistoric magma plumbing systems. J. Volcanol. and Geother. Res. 217–218, 73–90. https://doi.org/10.1016/j.jvolgeores.2011.12.014.

Hildner, E., Klügel, A., Hauff, F., 2011. Magma storage and ascent during the 1995 eruption of Fogo, Cape Verde archipelago. Contrib. Mineral. Petrol. 162, 751–772. https://doi.org/10.1007/s00410-011-0623-6.

Hoernle, K., Tilton, G., Le Bas, M.J., Duggen, S., Garbe-Schönberg, D., 2002. Geochemistry of oceanic carbonatites compared with continental carbonatites: mantle recycling of oceanic crustal carbonate. Contrib. Min. Petrol. 142, 520–542. https://doi.org/10.1007/s004100100308.

Hoernle, K., Werner, R., Morgan, J.P., Garbe-Schönberg, D., Bryce, J., Mrazek, J., 2000. Existence of complex spatial zonation in the Galápagos plume. Geology 28, 435. https://doi.org/10.1130/0091-7613(2000)28<435:EOCSZI>2.0.CO;2.

Hoggard, M.J., Parnell-Turner, R., White, N., 2020. Hotspots and mantle plumes revisited: towards reconciling the mantle heat transfer discrepancy. Earth Planet. Sci. Lett. 542, 116317 https://doi.org/10.1016/j.epsl.2020.116317.

Iacono-Marziano, G., Morizet, Y., Le Trong, E., Gaillard, F., 2012. New experimental data and semi-empirical parameterization of H_2O–CO_2 solubility in mafic melts. Geochim. Cosmochim. Acta 97, 1–23. https://doi.org/10.1016/j.gca.2012.08.035.

Iacono-Marziano, G., Paonita, A., Rizzo, A., Gaillard, F., Scaillet, B., 2010. Noble gas solubility in silicate melts: new experimental results and a comprehensive model of the effects of liquid composition, temperature and pressure. Chem. Geol. 279, 145–157. https://doi.org/10.1016/j.chemgeo.2010.10.017.

Jackson, M.G., Dasgupta, R., 2008. Compositions of HIMU, EM1, and EM2 from global trends between radiogenic isotopes and major elements in ocean island basalts. Earth Planet. Sci. Lett. 276, 175–186. https://doi.org/10.1016/j.epsl.2008.09.023.

Jackson, M.G., Konter, J.G., Becker, T.W., 2017a. Primordial helium entrained by the hottest mantle plumes. Nature 542, 340–343. https://doi.org/10.1038/nature21023.

Jackson, M.G., Price, A.A., Blichert-Toft, J., Kurz, M.D., Reinhard, A.A., 2017b. Geochemistry of lavas from the Caroline hotspot, Micronesia: evidence for primitive and recycled components in the mantle sources of lavas with moderately elevated $^3He/^4He$. Chem. Geol. 455, 385–400. https://doi.org/10.1016/j.chemgeo.2016.10.038.

Jørgensen, J.Ø., Holm, P.M., 2002. Temporal variation and carbonatite contamination in primitive ocean island volcanics from São Vicente, Cape Verde Islands. Chem. Geol. 192, 249–267. https://doi:10.1016/S0009-2541(02)00198-5.

Kessel, R., Schmidt, M.W., Ulmer, P., Pettke, T., 2005. Trace element signature of subduction-zone fluids, melts and supercritical fluids at 120–180 km depths. Nature 437, 724–727.

Klügel, A., Day, S., Schmid, M., Faria, B., 2020. Magma plumbing during the 2014–2015 Eruption of Fogo (Cape Verde Islands). Front. Earth Sci. 8, 157. https://doi.org/10.3389/feart.2020.00157.

Klügel, A., Hoernle, K.A., Schmincke, H., White, J.D.L., 2000. The chemically zoned 1949 eruption on La Palma (Canary Islands): petrologic evolution and magma supply dynamics of a rift zone eruption. J. Geophys. Res. 105, 5997–6016. https://doi.org/10.1029/1999JB900334.

Kurz, M.D., 1986. Cosmogenic helium in a terrestrial igneous rock. Nature 320, 435–439. https://doi.org/10.1038/320435a0.

Kurz, M.D., Kenna, T.C., Lassiter, J.C., DePaolo, D.J., 1996. Helium isotopic evolution of Mauna Kea Volcano: first results from the 1-km drill core. J. Geophys. Res. 101, 11781–11791. https://doi.org/10.1029/95JB03345.

Lo Forte, F.M., Aiuppa, A., Rotolo, S.G., Zanon, V., 2023. Temporal evolution of the Fogo Volcano magma storage system (Cape Verde Archipelago): a fluid inclusions perspective. J. Volcanol. Geotherm. Res. 433, 107730 https://doi.org/10.1016/j.jvolgeores.2022.107730.

Lo Forte, F.M., Schiavi, F., Rose-Koga, E.F., Rotolo, S., Verdier-Paoletti, M., Aiuppa, A., et al., 2024. High CO_2 in the mantle source of ocean island basanites. Geochim. Cosmochim. Acta 368, 93–111. https://doi.org/10.1016/j.gca.2024.01.016.

Lodge, A., Helffrich, G., 2006. Depleted swell root beneath the Cape Verde Islands. Geology 34, 449. https://doi.org/10.1130/G22030.1.

Macpherson, C.G., Mattey, D.P., 1994. Carbon isotope variations of CO_2 in Lau Basin basalts and ferrobasalts. Earth Planet. Sci. Lett. 121, 263–276. https://doi.org/10.1016/0012- 21X(94)90072-8.

Martins, S., Mata, J., Munhá, J., Mendes, M.H., Maerschalk, C., Caldeira, R., Mattielli, N., 2010. Chemical and mineralogical evidence of the occurrence of mantle metasomatism by carbonate-rich melts in an oceanic environment (Santiago Island, Cape Verde). Miner. Petrol. 99, 43–65. https://doi.org/10.1007/s00710-009-0078-x.

Marty, B., 2012. The origins and concentrations of water, carbon, nitrogen and noble gases on Earth. Earth Planet. Sci. Lett. 313–314, 56–66. https://doi.org/10.1016/j.epsl.2011.10.040.

Mata, J., Martins, S., Mattielli, N., Madeira, J., Faria, B., Ramalho, R.S., Silva, P., Moreira, M., Caldeira, R., Moreira, M., Rodrigues, J., Martins, L., 2017. The 2014–15 eruption and the short-term geochemical evolution of the Fogo volcano (Cape Verde): evidence for small-scale mantle heterogeneity. Lithos 288–289, 91–107. https://doi.org/10.1016/j.lithos.2017.07.001.

Melián, G.V., Hernández, P.A., Pérez, N.M., Asensio-Ramos, M., Padrón, E., Alonso, M., Padilla, G.D., Barrancos, J., Sortino, F., Sumino, H., Rodríguez, F., Amonte, C., Silva, S., Cardoso, N., Pereira, J.M., 2021. Insights from fumarole gas geochemistry on the recent volcanic unrest of Pico do Fogo, Cape Verde. Front. Earth Sci. 9, 631190 https://doi.org/10.3389/feart.2021.631190.

Millet, M.A., Doucelance, R., Schiano, P., David, K., Bosq, C., 2008. Mantle plume heterogeneity versus shallow-level interactions: a case study, the São Nicolau Island, Cape Verde archipelago. J. Volcanol. Geotherm. Res. 176, 265–276. https://doi.org/10.1016/j.jvolgeores.2008.04.003.

Mourão, C., Mata, J., Doucelance, R., Madeira, J., da Silveira, A.B., Silva, L.C., et al., 2010. Quaternary extrusive calciocarbonatite volcanism on Brava Island (Cape Verde): a nephelinite-carbonatite immiscibility product. J. Afr. Earth Sci. 56 (2), 59–74. https://doi.org/10.1007/s00410-011-0711-7.

Mourão, C., Moreira, M., Mata, J., Raquin, A., Madeira, J., 2012. Primary and secondary processes constraining the noble gas isotopic signatures of carbonatites and silicate rocks from Brava Island: evidence for a lower mantle origin of the Cape Verde plume. Contrib. Mineral. Petrol. 163, 995–1009. https://doi.org/10.1007/s00410-011-0711-7.

Ozima, M., Podosek, F.A., 2002. Noble Gas Geochemistry. Cambridge Univ. Press, Cambridge. https://doi.org/10.1017/CBO9780511545986 ed. 2.

Pim, J., Peirce, C., Watts, A.B., Grevemeyer, I., Krabbenhoeft, A., 2008. Crustal structure and origin of the Cape Verde Rise. Earth Planet. Sci. Lett. 272, 422–428. https://doi.org/10.1016/j.epsl.2008.05.012.

Pineau, F., Mathez, E.A., 1990. Carbon isotopes in xenoliths from the Hualalai Volcano, Hawaii, and the generation of isotopic variability. Geochim. Cosmochim. Acta 54, 217–227. https://doi.org/10.1016/0016-7037(90)90209-4.

Putirka, K.D., 2008. Thermometers and Barometers for Volcanic Systems. Rev. Mineral. Geochem. 69, 61–120. https://doi.org/10.2138/rmg.2008.69.3.

Ramalho, R.A.S., 2011. Building the Cape Verde Islands. Springer Berlin Heidelberg, Berlin, Heidelberg. https://doi.org/10.1007/978-3-642-19103-9.

Remigi, S., Frezzotti, M.L., Rizzo, A.L., Esposito, R., Bodnar, R.J., Sandoval-Velasquez, A., et al., 2023. Spatially resolved CO_2 carbon stable isotope analyses at the microscale using Raman spectroscopy. Sci. Rep. 13, 18561. https://doi.org/10.1038/s41598-023-44903-z.

Rizzo, A.L., Barberi, F., Carapezza, M.L., Di Piazza, A., Francalanci, L., Sortino, F., D'Alessandro, W., 2015. New mafic magma refilling a quiescent volcano: evidence from He-Ne-Ar isotopes during the 2011-2012 unrest at Santorini. Greece Geochem. Geophys. Geosyst. 16, 798–814. https://doi.org/10.1002/2014GC005653.

Rizzo, A.L., Caracausi, A., Chavagnac, V., Nomikou, P., Polymenakou, P.N., Mandalakis, M., Kotoulas, G., Magoulas, A., Castillo, A., Lampridou, D., Marusczak, N., Sonke, J.E., 2019. Geochemistry of CO_2-rich gases venting from

submarine volcanism: the case of Kolumbo (Hellenic Volcanic Arc, Greece). Front. Earth Sci. 7, 60. https://doi.org/10.3389/feart.2019.00060.
Rizzo, A.L., Di Piazza, A., de Moor, J.M., Alvarado, G.E., Avard, G., Carapezza, M.L., Mora, M.M., 2016. Eruptive activity at Turrialba volcano (Costa Rica): inferences from 3He/4He in fumarole gases and chemistry of the products ejected during 2014 and 2015. Geochem. Geophys. Geosyst. 17, 4478–4494. https://doi.org/10.1002/2016GC006525.
Rizzo, A.L., Faccini, B., Casetta, F., Faccincani, L., Ntaflos, T., Italiano, F., Coltorti, M., 2021. Melting and metasomatism in West Eifel and Siebengebirge sub-continental lithospheric mantle: evidence from concentrations of volatiles in fluid inclusions and petrology of ultramafic xenoliths. Chem. Geol. 581, 120400 https://doi.org/10.1016/j.chemgeo.2021.120400.
Rizzo, A.L., Pelorosso, B., Coltorti, M., Ntaflos, T., Bonadiman, C., Matusiak-Małek, M., Italiano, F., Bergonzoni, G., 2018. Geochemistry of noble gases and CO_2 in fluid inclusions from lithospheric mantle beneath Wilcza Góra (Lower Silesia, Southwest Poland). Front. Earth Sci. 6, 215. https://doi.org/10.3389/feart.2018.00215.
Sandoval-Velasquez, A., Rizzo, A.L., Aiuppa, A., Remigi, S., Padrón, E., Pérez, N.M., Frezzotti, M.L., 2021a. Recycled crustal carbon in the depleted mantle source of El Hierro volcano, Canary Islands. Lithos 400–401, 106414. https://doi.org/10.1016/j.lithos.2021.106414.
Sandoval-Velasquez, A., Rizzo, A.L., Frezzotti, M.L., Saucedo, R., Aiuppa, A., 2021b. The composition of fluids stored in the central Mexican lithospheric mantle: inferences from noble gases and CO_2 in mantle xenoliths. Chem. Geol. 576, 120270 https://doi.org/10.1016/j.chemgeo.2021.120270.
Sandoval-Velasquez, A., Rizzo, A.L., Casetta, F., Ntaflos, T., Aiuppa, A., Alonso, M., Padrón, E., Pankhurst, M.J., Mundl-Petermeier, A., Zanon, V., Pérez, N.M., 2023. The noble gas signature of the 2021 Tajogaite eruption (La Palma, Canary Islands). J. Volcanol. Geotherm. Res. 443, 107928 https://doi.org/10.1016/j.jvolgeores.2023.107928.
Sandoval-Velasquez, A., Casetta, F., Ntaflos, T., Aiuppa, A., Coltorti, M., Frezzotti, M.L., et al., 2024. 2021 Tajogaite eruption records infiltration of crustal fluids within the upper mantle beneath La Palma, Canary Islands. Front. Earth Sci. 12, 1303872. https://doi:10.3389/feart.2024.1303872.
Sano, Y., Marty, B., 1995. Origin of carbon in fumarolic gas from island arcs. Chem. Geol. 119, 265–274. https://doi.org/10.1016/0009-2541(94)00097-R.
Schutt, D.L., Lesher, C.E., 2006. Effects of melt depletion on the density and seismic velocity of garnet and spinel lherzolite: melt depletion. J. Geophys. Res. 111 https://doi.org/10.1029/2003JB002950 n/a-n/a.
Stracke, A., Bourdon, B., 2009. The importance of melt extraction for tracing mantle heterogeneity. Geochim. Cosmochim. Acta 73, 218–238. https://doi:10.1016/j.gca.2008.10.015.
Stracke, A., Genske, F., Berndt, J., Koornneef, J.M., 2019. Ubiquitous ultra-depleted domains in Earth's mantle. Nat. Geosci. 12, 851–855. https://doi.org/10.1038/s41561-019-0446-z.
Sun, C., Dasgupta, R., 2023. Carbon budget of Earth's deep mantle constrained by petrogenesis of silica-poor ocean island basalts. Earth Planet. Sci. Lett. 611, 118135 https://doi.org/10.1016/j.epsl.2023.118135.
Van Gerve, T.D., Neave, D.A., Wieser, P., Lamadrid, H., Hulsbosch, N., Namur, O., 2024. The origin and differentiation of CO_2-rich primary melts in ocean island volcanoes: integrating 3D X-Ray tomography with chemical microanalysis of olivine-hosted melt inclusions from Pico (Azores). J. Petrol. 65 (2), egae006. https://doi.org/10.1093/petrology/egae006.
Vinnik, L., Silveira, G., Kiselev, S., Farra, V., Weber, M., Stutzmann, E., 2012. Cape Verde hotspot from the upper crust to the top of the lower mantle. Earth Planet. Sci. Lett. 319–320, 259–268. https://doi.org/10.1016/j.epsl.2011.12.017.
Wilson, D., Peirce, C., Watts, A., Grevemeyer, I., 2013. Uplift at lithospheric swells—II: is the Cape Verde mid-plate swell supported by a lithosphere of varying mechanical strength? Geophys. J. Int. 193, 798–819. https://doi.org/10.1093/gji/ggt034.
Zindler, A., Hart, S., 1986. Chemical geodynamics. Annu. Rev. Earth Planet. Sci. 14, 493–571. https://doi.org/10.1146/annurev.ea.14.050186.002425.

Further readings

Hilton, D.R., Fischer, T.P., Marty, B., 2002. Noble gases and volatile recycling at subduction zones. Rev. Min. Geochem. 47, 319–370. https://doi.org/10.2138/rmg.2002.47.9.
Liu, X., Zhao, D., 2021. Seismic evidence for a plume-modified oceanic lithosphere–asthenosphere system beneath Cape Verde. Geophys. J. Int. 225, 872–886. https://doi.org/10.1093/gji/ggab012.
Pollitz, F.F., 1991. Two-stage model of African absolute motion during the last 30 million years. Tectonophysics 194, 91–106. https://doi.org/10.1016/0040-1951(91)90274-V.